

A cell type-specific mechanism driving the rapid antidepressant effects of transcranial magnetic stimulation

Michael W. Gongwer^{1,2,3}, Alex Qi⁴, Alexander S. Enos¹, Sophia A. Rueda Mora¹, Cassandra B. Klune¹, Meelan Shari¹, Adrienne Q. Kashay⁴, Owen H. Williams¹, Aliza Hacking¹, Jack P. Riley¹, Gary A. Wilke, Yihong Yang⁵, Hanbing Lu⁵, Andrew F. Leuchter⁴, Laura A. DeNardo^{1*}, Scott A. Wilke^{4*}

Affiliations:

¹Department of Physiology, David Geffen School of Medicine, University of California, Los Angeles; Los Angeles, CA 90095, USA

²Neuroscience Interdepartmental Program, David Geffen School of Medicine, University of California, Los Angeles; Los Angeles, CA 90095, USA

³Medical Scientist Training Program, David Geffen School of Medicine, University of California, Los Angeles; Los Angeles, CA 90095, USA

⁴Semel Institute for Neuroscience and Human Behavior, Department of Psychiatry, Neuromodulation Division, David Geffen School of Medicine, University of California, Los Angeles; Los Angeles, CA 90095, USA

⁵Neuroimaging Research Branch, National Institute on Drug Abuse, Intramural Research Program, National Institutes of Health, Baltimore, MD 21224, USA

*Correspondence:

Dr. Scott Wilke, 760 Westwood Plaza, Semel Institute Rm. #57-438, David Geffen School of Medicine at UCLA, Los Angeles, CA 90024 - swilke@mednet.ucla.edu

Dr. Laura DeNardo, 650 Charles E Young Dr. S, Center for Health Sciences Rm. #77200A, David Geffen School of Medicine at UCLA, Los Angeles, CA 90095 - ldenardo@ucla.edu

Abstract: Repetitive transcranial magnetic stimulation (rTMS) is an emerging treatment for brain disorders, but its therapeutic mechanism is unknown. We developed a novel mouse model of rTMS with superior clinical face validity and investigated the neural mechanism by which accelerated intermittent theta burst stimulation (aiTBS) – the first rapid-acting rTMS antidepressant protocol – reversed chronic stress-induced behavioral deficits. Using fiber photometry, we showed that aiTBS drives distinct patterns of neural activity in intratelencephalic (IT) and pyramidal tract (PT) projecting neurons in dorsomedial prefrontal cortex (dmPFC). However, only IT neurons exhibited persistently increased activity during both aiTBS and subsequent depression-related behaviors. Similarly, aiTBS reversed stress-related loss of dendritic spines on IT, but not PT neurons, further demonstrating cell type-specific effects of stimulation. Finally, chemogenetic inhibition of dmPFC IT neurons during rTMS blocked the antidepressant-like behavioral effects of aiTBS. Thus, we demonstrate a prefrontal mechanism linking rapid aiTBS-driven therapeutic effects to cell type-specific circuit plasticity.

42 Introduction

44 Brain stimulation promises to revolutionize treatment of brain disorders characterized by aberrant
46 circuit function¹. Transcranial magnetic stimulation (TMS) is a non-invasive form of focal
48 neuromodulation that drives neural activity in a target region using electromagnetic pulses²⁻⁴.
50 TMS is the dominant form of clinical brain stimulation used to treat depression and a number of
52 other disorders⁵⁻⁸. When employed to treat neuropsychiatric disorders, repetitive TMS (rTMS)
pulse sequences are used to produce lasting changes in brain function^{9,10}. While this is often
effective, many patients fail to respond or have residual symptoms^{11,12}, and several brain
disorders do not have approved rTMS-based therapies. The lack of a mechanistic understanding
of rTMS impedes the rational optimization of protocols that target dysfunctional circuits underlying
specific symptoms or disorders.

54 Prefrontal cortex (PFC) dysfunction is a hallmark of major depressive disorder^{13,14}. In clinical
56 rTMS, the coil is targeted to specific cortical regions based on theories about the brain networks
58 disrupted in a particular disorder¹⁵⁻¹⁷. While work from preclinical models has suggested that
60 rTMS may drive plasticity in specific cortical cell types¹⁸⁻²², no studies to date have identified
62 causal mechanisms driving changes in behavior. As a result, it remains unclear whether rTMS
64 drives lasting therapeutic effects by modifying specific cell types or circuits within the clinical target
66 region *in vivo*. Progress towards discovering these circuit mechanisms has been limited by a lack
of preclinical animal models of rTMS with strong face validity for how rTMS is delivered clinically.
Recently, a prefrontal-targeted, accelerated intermittent theta burst stimulation (aiTBS) rTMS
protocol, which compresses a typical 6-week treatment course to just 5 days, has been shown to
rapidly reverse symptoms of depression and produce long-lasting effects²³⁻²⁵. Here we developed
a novel preclinical model of rTMS and used it to discover how aiTBS drives cell-type specific
plasticity in PFC *in vivo*.

68 Results

68 Establishing a novel preclinical rodent model of rTMS

70 In order to study the circuit mechanisms underlying the therapeutic effects of rTMS, we needed a
72 rodent model that allowed us to deliver clinically effective protocols and mimicked how patients
74 are treated with TMS in the clinic. However, scaling rTMS coils to the smaller rodent brain poses
76 significant challenges^{26,27}. Prior preclinical models used anesthetized mice and oversized coils
78 that likely stimulated most of the brain, or miniaturized coils that were too weak to elicit action
80 potentials²⁸⁻³³. Our group recently developed and extensively validated a novel coil design that
82 overcomes these limitations, enabling highly focal (<2mm), suprathreshold stimulation of a
cortical subregion in the rodent brain³⁴⁻³⁷. Using this coil, we developed a system that enables us
to combine delivery of clinical rTMS protocols with rigorous investigation of neural circuit
mechanisms in the awake mouse (Fig. 1A). Our model mimics how TMS patients are treated in
the clinic, with the head held stable and in an awake state. Indeed, rTMS delivered under
anesthesia can have effects that are opposite of those observed in awake animals, underscoring
the translational importance of brain state²⁸.

84 We first verified the focality of stimulation in the awake mouse brain. To do so, we measured
86 evoked motor responses when the coil hotspot – the location of the sharply focused electric field
88 – was positioned over the hindlimb region of the primary motor cortex. Single pulses delivered to
90 this region, which spans approximately 1 mm² in the mouse brain^{38,39}, elicited tightly time-locked
motor responses limited to the contralateral hindlimb, confirming highly focal, suprathreshold
stimulation (Fig. 1B,C). This is consistent with our previous reports, using the same coil, which
used activity-dependent labeling and motor-evoked potentials to demonstrate similar focality^{34,35}.
To ensure precise and reliable positioning of the coil hotspot, we marked the region to be

92 stimulated using stereotaxic coordinates. The TMS coil was mounted on a fine 3-axis manipulator
to allow precise targeting in head-fixed mice that were freely running on a wheel (Fig. 1A).

94
95 While high-frequency clinical protocols are the most commonly used protocols in patients, they
96 have been difficult to model in rodents because miniaturized coils tend to easily overheat²⁶. To
97 overcome this challenge, we surrounded our coil with a custom-designed, liquid-cooled heatsink,
98 which allowed us to efficiently deliver longer clinical protocols (Fig. 1A). The coil was connected
to a FDA-approved clinical stimulator capable of delivering theta burst protocols, which more
100 efficiently elicit effects at lower stimulation intensities⁴⁰. We utilized a recently developed aiTBS
clinical protocol which targets the PFC to rapidly reverse depressive symptoms^{23,24,41}. Our
102 experiments used 1800 pulses of iTBS deployed as 10 sessions occurring once every hour,
identical to the clinical protocol effective in patients (Fig. 1D)^{23,24,41}. We delivered rTMS and sham
104 treatment simultaneously, using identical side-by-side setups (Fig. S1).

106 **aiTBS reverses the behavioral effects of chronic stress**

Depression is a highly pleiotropic condition driven by both environmental and genetic factors.
108 Chronic stress is a major risk factor for depression and other psychiatric disorders^{42,43}. Animal
models of chronic stress reliably induce dendritic spine loss, dorsomedial PFC (dmPFC)
110 hypofunction and other cellular and circuit disturbances^{44–47}. These changes are thought to disrupt
core functions of dmPFC including motivation, effort-reward valuation, and decision-making,
112 manifesting as disordered behavior^{46,47}. Patients suffering from depression often exhibit
symptoms that are thought to arise from these deficits, including low resilience in the face of acute
114 stressors^{42,48}. Recently, interventions such as ketamine and psychedelic compounds have been
shown to produce rapid-acting antidepressant behavioral effects by reversing the neurobiological
116 disturbances generated by chronic stress^{46,49,50}. We hypothesized that an accelerated rTMS
protocol like aiTBS may elicit similar changes.

118
To better understand how rTMS drives antidepressant effects, we applied our novel rodent TMS
120 system to a mouse model of chronic stress. We modeled the effects of stress using a well-
validated protocol: chronic administration of the steroid hormone corticosterone (CORT; Fig.
122 1E)^{46,47,51–53}. Then, using a series of behavioral tests, we examined how mice responded when
exposed to acutely stressful situations. CORT reliably increased passive coping (immobility) in
124 the forced swim test (FST), consistent with the decreased effortful persistence characteristic of a
depression-like behavioral state (Fig. 1F). To ensure these behavioral effects were robust, we
126 repeated these experiments using a different chronic stress protocol in which mice are exposed
to a series of environmental stressors (unpredictable chronic mild stress; UCMS)^{54,55}. Similar to
128 CORT, mice that experienced UCMS exhibited increased immobility in the FST (Fig. 1F).

130 Depression is highly comorbid with anxiety, and rTMS can improve symptoms of both^{56,57}.
Therefore, we also examined how CORT impacted behavior in two commonly used assays for
132 anxiety-like behaviors in rodents: the elevated zero maze (EZM) and open field test (OFT). The
EZM and OFT measure how much time mice spend in exposed parts of an apparatus, where they
134 are more vulnerable to predation. CORT decreased the time spent in the open arms of the EZM,
suggesting an increase in anxiety-like behavior (Fig. 1G). We found no behavioral effects of
136 CORT in the OFT, which has less physical distinction between the safe and vulnerable areas of
the arena compared to EZM (Fig. 1H). Thus, chronic CORT produced a behavioral state with
138 anxiety- and depression-like features, which we could use to interrogate the potential therapeutic
mechanisms underlying rTMS treatment of depression.

140
141 We hypothesized that aiTBS targeting dmPFC would reverse behavioral deficits observed in our
142 CORT model of chronic stress. To test this, mice were placed on CORT, treated with aiTBS (10

144 aiTBS sessions in 1 day), and then assessed for behavioral outcomes the following day (Fig. 1I).
145 aiTBS treatment significantly reduced immobility in the FST compared to sham-treated controls
146 (Fig. 1J), consistent with an antidepressant-like effect. We also observed strong trends toward
147 increased time in the open arms of the EZM and in the center of the OFT following aiTBS
148 treatment (Fig. 1K,L). To examine the overall response to aiTBS across these assays, we
149 calculated a composite score based on behavior in the FST, EZM, and OFT. The results indicated
150 that aiTBS significantly improved anxiety- and depression-like behaviors (Fig. 1M). We also
151 replicated the effects of aiTBS on FST behavior in mice exposed to UCMS instead of CORT (Fig.
152 S2). Thus, our model exhibits strong face validity for clinical rTMS and recapitulates the rapid
therapeutic effects seen with accelerated rTMS for depression.

154 Chronic stress models of depression are also characterized by other behavioral features,
155 including anhedonia and reduced effortful persistence⁵⁸⁻⁶⁰. We used additional assays to test
156 whether our novel model of aiTBS could ameliorate such behavioral impairments. We used the
157 sucrose preference test (SPT) to measure behavioral anhedonia⁶¹, a proposed corollary of the
158 reduced ability to experience pleasure which is a core feature of depression⁵⁸. Chronic CORT
159 administration decreased sucrose preference from a pre-stress baseline, and aiTBS reversed this
160 effect (Fig. S3A-C). As an additional measure of effortful behavioral persistence beyond the FST,
161 we used the sinking platform test⁶⁰. This assay measures the propensity to retain goal-directed
162 actions under adverse conditions (Fig. S3D-E). Chronic CORT decreased behavioral persistence
163 (measured as the number of platforms climbed), and aiTBS reversed this effect (Fig. S3F-H).
164 These findings indicate that dmPFC-targeted aiTBS improves the behavioral consequences of
165 chronic stress related to both anhedonia and behavioral persistence.

166 Clinical depression is frequently characterized by imbalances in the drive to approach rewarding
167 stimuli and avoid aversive stimuli⁶², leading to maladaptive decision-making in the face of
168 approach-avoidance conflicts⁶². We therefore evaluated the effects of aiTBS on stress-induced
169 disruptions in the balance of reward approach and threat avoidance behaviors. We used an
170 approach-avoidance conflict assay where mice must balance approaching a liquid reward with
171 avoiding a cued footshock (Fig. S4A-C)⁶³. Mice must balance approach and avoidance behaviors
172 during periods of elevated threat (tone), or relative safety during inter-tone intervals (ITI). Across
173 training, mice from all experimental groups displayed similar increases in avoidance and
174 reductions in reward-seeking during the tone period (Fig. S4D). By the end of training and during
175 a retrieval session without foot shocks, stressed, aiTBS-treated and non-stressed control mice
176 had a significantly higher adaptive preference for the reward zone during the ITI compared to
177 stressed, sham-treated mice (Fig. S4E-G). Therefore, aiTBS reversed the stress-induced
178 decreases in reward-seeking behavior during approach-avoidance conflict. These changes were
179 specific to intervals when the threatening cue was absent, when approach was adaptive and
180 avoidance was maladaptive. Taken together, these findings demonstrate that a clinically effective
181 aiTBS protocol can rapidly reverse multiple stress-induced behavioral deficits relevant to
182 depression.

184 **aiTBS elicits cell type-specific neuromodulation**

186 Having developed an experimentally tractable system for studying rTMS, we sought to discover
187 the neural mechanisms underlying the therapeutic behavioral effects of aiTBS. Patients suffering
188 from depression exhibit reduced motivation to exert effort, excessive avoidance of aversive stimuli
189 and altered encoding of emotional stimuli in PFC, amongst other deficits⁶⁴. Thus, effective
190 treatment with aiTBS likely alters activity in the cell types and circuits that underlie these
191 behavioral changes. Within dmPFC, projection-defined classes of neurons play distinct roles in
192 behavior, and manipulating these projections can produce distinct effects in the FST and other
depression-related behaviors⁶⁵⁻⁷⁰. The PFC contains intratelencephalic (IT) and pyramidal tract

194 (PT) projection classes^{71,72}, two non-overlapping excitatory cell types that are defined by their
196 long-range projection targets and are highly conserved across species and between cortical
198 regions^{73,74}. IT neurons project to cortical and striatal targets, while PT neurons project to
198 midbrain, hindbrain, striatal, and thalamic targets^{73,74}. dmPFC IT and PT neurons receive
200 markedly distinct local and long-range synaptic inputs and exhibit unique molecular profiles^{75–79}.
202 Growing evidence suggests that imbalanced IT/PT function in PFC may underlie neuropsychiatric
204 disease states, including depression⁸⁰. Thus, we hypothesized that IT and PT neurons may
206 differentially respond to aiTBS and/or play distinguishable roles in the therapeutic effects of
208 aiTBS. To test this, we recorded IT and PT neuronal activity during iTBS, followed by recording
210 during effortful coping and encoding of appetitive and aversive stimuli.

204 We reasoned that if we could detect differential effects of aiTBS on IT and PT neuron activity, this
206 would generate insight into the loci of rTMS-driven circuit plasticity. To investigate this, we first
208 used fiber photometry to record activity of dmPFC IT and PT neurons expressing the genetically
210 encoded calcium sensor GCaMP7f (Fig. 2A-C, S5). We developed a surgical approach to implant
212 the optical fiber from the side of the brain, allowing simultaneous rTMS delivery and recording of
214 neural activity (Fig. 2B). After mice received chronic CORT treatment, we measured how IT and
216 PT neurons acutely responded during aiTBS (Fig. 2D).

212 For each mouse, we recorded GCaMP fluorescence (a proxy for neural activity) during the first
214 10-minute aiTBS session. When normalized to the pre-train period, iTBS elicited a ramping
216 increase in activity for both IT and PT neurons, which persisted for at least 4 seconds into the
218 intertrain interval (Fig. 2E,F). For IT neurons, the GCaMP fluorescence signal remained elevated
220 in aiTBS-treated but not sham-treated mice for 4-8 seconds after stimulation onset, whereas
222 activity in PT neurons dropped back to baseline during this period (Fig. 2E,F). To determine how
224 the overall magnitude of signals arising from IT and PT neurons changed, we normalized
226 fluorescence activity during aiTBS to the corresponding sham signals and plotted the activity
228 across the entire 10-minute aiTBS session for each cell type (Fig. 2G). IT neurons in aiTBS-
230 treated mice exhibited increased activity relative to sham-treated mice throughout the 10-minute
232 aiTBS session, whereas PT neurons exhibited a trend in the opposite direction (Fig. 2H). Thus,
234 aiTBS elicits distinct activity patterns in prefrontal IT and PT cells.

226 We hypothesized that the prolonged increase in IT neuron activity during an aiTBS session may
228 potentiate activity in IT circuits to ameliorate depression-like behavior. To test this, on the day
230 following aiTBS treatment, we used fiber photometry to record signals from dmPFC neurons
232 during bouts of effortful activity in the tail suspension test (TST; Fig. 3A). We used this assay
234 because the lateralized fiber optic placement was incompatible with the tight walls of the FST and
236 other assays. Like the FST, the TST also measures effortful coping in response to an inescapable
238 acute stressor. During the TST, IT neurons exhibited significantly higher activity at the onset of
240 struggling epochs in aiTBS-treated compared to sham-treated mice (Fig. 3B-E). In aiTBS-treated
242 mice, ramping IT neuron activity was evident even before the onset of struggling bouts (Fig. 3D).
244 Moreover, there was enhanced IT activity from the onset of effortful struggling behavior to at least
246 15 seconds afterward (Fig. 3E). In contrast, there was no lasting effect of aiTBS on PT neuron
248 activity associated with the onset of struggling bout (Fig. 3B). We did not observe any significant
250 changes in activity at struggling offset in either cell type (Fig. 3C).

240 Based on these findings, we hypothesized that aiTBS may modulate how strongly IT or PT
242 neurons encode effortful stress coping responses. To test this, we fit a generalized linear model
244 to examine the predictive relationship between the cell type-specific activity and an automated
246 measure of struggling vigor for each mouse. aiTBS-treated animals exhibited an increase in the
248 strength of the correlation between neural signals and struggling vigor for IT, but not PT neurons

246 (Fig. 3F). Altogether, these results demonstrate that aiTBS drives plasticity in IT neurons that enhances IT neuronal activity during effortful coping behavior.

248 We next investigated whether the effects of aiTBS on IT and PT neuronal activity were specific to
250 effortful coping or generalized to other behavioral responses. To test this, we recorded GCaMP
252 fluorescence from IT and PT neurons during the OFT, which had walls wide enough to be
254 compatible with the lateral fiber. Compared to sham-treated mice, aiTBS-treated mice had
256 elevated IT neuron activity preceding entries to and following exits from the center of the arena
(Fig. 3G-J). In contrast, aiTBS did not drive changes in PT neuron activity in either case.
Consistent with our TST results, these data suggest that aiTBS alters IT, but not PT, activity-
behavior relationships in a manner that may ameliorate depression- and anxiety-related
behaviors.

258 dmPFC projection neurons, including those that fall within IT and PT classes, differentially encode
aversive and rewarding stimuli and can bias approach or avoidance of these stimuli through top-
260 down control of downstream brain regions⁸¹. Chronic stress can lead to pathological processing
of emotional stimuli that manifests in mood and anxiety disorders^{64,82}. We hypothesized that
262 altered encoding of such stimuli may contribute to the effects of aiTBS on conflicting reward
approach and threat avoidance behaviors (Fig. S4). Because the lateralized fiber implant impeded
264 locomotion in the tight arena of the conflict assay, we instead used a head-fixed setup to present
mice with cues that predicted an aversive or rewarding stimulus while recording activity from IT
266 or PT neurons (Fig. S6). We did not observe any effect of aiTBS on IT or PT neuronal activity
during either stimulus. This suggests that the aiTBS-driven behavioral effects are not a direct
268 consequence of altered IT response to rewarding or aversive stimuli. This result further indicates
that aiTBS does not universally increase IT neuron activity, but rather enhances engagement of
270 IT neurons during specific depression-relevant behaviors.

272 **aiTBS reverses stress-related dendritic spine deficits in a cell type-specific manner**

Converging evidence indicates that synaptic remodeling underlies both the emergence of
274 depression and its resolution with effective treatment⁸³. Atrophy of prefrontal dendritic structure,
including decreased density of dendritic spines and postsynaptic proteins is a hallmark finding in
276 depression⁸⁴. These changes are recapitulated in rodent models of chronic stress^{44,45}, and mPFC
spine loss correlates with deficits in behaviors that require mPFC^{85,86}. Effective antidepressant
278 therapies can augment synapse function, promote new synapse formation and restore lost
dendritic spines^{49,83,87-89}. In some cases, dendritic spine elaboration is required for antidepressant
280 behavioral responses⁴⁶. Spine elaboration is an activity-dependent process, downstream of
excitatory synaptic plasticity mechanisms proposed to mediate the effects of rTMS^{9,18,19,90-95}.

282 We hypothesized that aiTBS-driven elaboration of dendritic spines may underlie the increased
284 activity we observed in IT neurons during depression-related behavior. To explore this, we used
a viral-genetic strategy⁹⁶ to sparsely and brightly label the dendrites of either IT or PT neurons
286 (Fig. 4A). Mice with cell type-specific labeling were exposed to chronic CORT and treated with
aiTBS. We then imaged fluorescently labeled dmPFC IT and PT neurons using confocal
288 microscopy (Fig. 4B,C) and quantified spine density on apical and basal dendrites, which receive
synaptic input from distinct sources⁹⁷ (Fig. 4D-G).

290 Mice exposed to chronic CORT exhibited reduced dendritic spine density on both IT and PT
292 neurons compared to non-stressed controls (Fig. 4D-G). In IT neurons, aiTBS treatment partially
reversed loss of dendritic spines on both apical and basal dendrites (Fig. 4E). In contrast, aiTBS
294 had no effect on PT neuron spine density (Fig. 4G), indicating that aiTBS-driven spine elaboration
was specific to IT neurons. These data suggest that, like other rapid-acting antidepressant

296 manipulations^{46,49,87–89}, aiTBS may drive activity-dependent processes that promote restoration of
298 lost dendritic spines. Our data further indicate that the effects of aiTBS are cell type-specific and
300 could reflect strengthening or restoration of lost synaptic inputs onto IT neurons, potentially
302 augmenting IT neuron engagement and IT circuit-mediated behavioral functions.

300 **Suppressing the activity of IT neurons during aiTBS blocks its antidepressant behavioral** 302 **effect**

304 Our findings suggest IT neurons are uniquely responsive to aiTBS, showing increased activity
306 over the course of a stimulation session and enhanced activity the following day. Thus, we
308 hypothesized that activation of these neurons during aiTBS may be necessary for subsequent
310 changes in depression-related behavior. To test this, we used chemogenetics to selectively
312 suppress IT neuron activity during aiTBS. We first expressed the inhibitory DREADD (designer
314 receptor exclusively activated by designer drugs) hM4Di⁹⁸ specifically in dmPFC IT neurons (Fig.
316 5A, S7). We then injected mice with the hM4Di ligand clozapine-N-oxide (CNO) to suppress the
318 activity of these neurons during aiTBS. To evaluate the effectiveness of this strategy, we injected
320 a subset of mice with CNO prior to a single 10-minute aiTBS session. Afterwards, we examined
322 expression of the immediate early gene Fos, a marker of recent neuronal activity (Fig. 5B). In
324 mice injected with CNO, we observed an ~75% reduction in Fos expression in hM4Di-expressing
326 IT neurons compared to mCherry-only controls (Fig. 5B). This indicates that our chemogenetic
328 manipulation effectively suppressed aiTBS-driven activity in IT neurons.

330 Next, to test whether IT activation is required to generate the antidepressant effects of aiTBS, we
332 chemogenetically suppressed activity in IT neurons throughout the entire course of aiTBS
334 treatment (Fig. 5C). In mCherry control animals, aiTBS but not sham treatment significantly
336 reduced immobility during the FST compared to the pre-TMS baseline (Fig. 5D). This aligns with
338 our previous behavioral effect in the FST and confirms that the effect is not eliminated by CNO
340 itself. In contrast, in mice expressing hM4Di in IT neurons, aiTBS did not affect immobility relative
342 to the pre-TMS baseline (Fig. 5D). In line with this, mice expressing hM4Di exhibited a smaller
344 change in immobility from pre to post aiTBS treatment compared to mCherry controls (Fig. 5E).
346 Thus, suppressing the activity of IT neurons during aiTBS treatment is sufficient to prevent
antidepressant-like changes in effortful coping behavior. Together our findings demonstrate that
clinical rTMS protocols such as aiTBS drive cell type-specific modifications in IT projection
neurons and aiTBS-driven activation of this projection class is required to reverse a behavioral
deficit associated with chronic stress.

332 **Discussion**

334 Non-invasive brain stimulation promises to treat brain disorders by resolving disturbances in
336 circuit function, but how specific circuits or cell types are affected is not known. Our study
338 establishes a novel rodent model of rTMS and sheds light on the cell type-resolved antidepressant
340 mechanism of aiTBS. We discovered that aiTBS, the first rapid rTMS protocol for depression,
342 rescues behavioral deficits induced by chronic stress via a cell type-specific neural mechanism.
Compared to PT cells, IT cells are uniquely sensitive to aiTBS, showing a gradual increase in
activity across a session. A single day of aiTBS restores lost dendritic spines and enhances neural
activity during effortful behavior in prefrontal IT, but not PT, neurons. Neural activity in local
prefrontal IT neurons is required during rTMS to produce the antidepressant-like behavioral
effects of aiTBS.

344 This study represents a significant advance in our understanding of how rTMS can modulate
346 specific cortical cell-types to produce clinically useful effects. Prior studies revealed that rTMS
modifies gene expression and produces structural and functional changes reminiscent of synaptic

348 long-term potentiation (LTP) or depression (LTD)^{18,19,99–101}. In some cases these effects were
350 specific to excitatory or inhibitory neurons^{18–22,102,103}. While important, these early studies were
352 based on models that lacked clinical face validity because they used non-clinical protocols,
354 anesthetized animals, were not focal and suprathreshold, or investigated non-clinical targets. Our
356 work overcomes these limitations and links cell-type specific neural activation during rTMS to
358 subsequent behavioral effects. IT and PT projection classes are a highly conserved circuit
architecture across cortical regions and between species^{73,74}. We find that IT neurons are uniquely
responsive to aiTBS-driven plasticity. Their unique response properties may arise as a function
of their specific local and long range connectivity, molecular expression profiles, or synaptic
properties^{72,75–79,104}. The extent to which each of these features contribute remains to be explored.
Our findings are highly consistent with a companion manuscript co-submitted with this report,
which provides additional evidence that aiTBS selectively modulates IT circuits¹⁰⁵.

360 There is growing interest in understanding the circuit changes that produce rapid resolution of
362 depression^{46,49,106,107}. Depression is characterized by heterogeneous disturbances in cognitive
364 and emotional brain networks that can arise at the intersection of genetic and environmental
366 factors, including chronic stress^{13,43,108,109}. It is important to note that rodent behavioral assays
368 cannot directly prove relevance to symptoms of depression, but we used assays that evoke
cognitive and emotional processes disrupted in chronic stress. The PFC is a critical hub in these
networks and is highly sensitive to chronic stress. Hypofunction of prefrontal projection neurons
and the resulting aberrant activity patterns are a point of convergence for factors that promote or
alleviate depressed states^{46,67,69}.

370 Our findings suggest IT neurons are a novel target for the development of precision medicine
372 interventions for depression and other conditions, by selective modulation using aiTBS or other
374 brain stimulation strategies. It is possible that different stimulation protocols, or combination of
376 rTMS with pharmacologic agents, will drive distinct effects, promoting plasticity in other cell types.
378 In the clinic, combining rTMS with modulation of dopaminergic and noradrenergic activity via
380 psychostimulants may enhance antidepressant outcomes^{110,111}. This suggests combination
382 therapy may promote plasticity in circuits that may not otherwise respond to rTMS. Beyond
depression, aiTBS and other rTMS protocols are being studied in the treatment of other
neurological and psychiatric disorders, including addiction, schizophrenia, dementia, and chronic
pain¹¹². Our work sets the foundation for the discovery of noninvasive cell-type specific treatment
protocols that are targeted to dysfunctional circuit elements of these unique symptoms and
disorders.

384 References

- 386 1. Rajasethupathy, P., Ferenczi, E., and Deisseroth, K. (2016). Targeting Neural Circuits. *Cell*
388 *165*, 524–534. <https://doi.org/10.1016/j.cell.2016.03.047>.
- 390 2. Barker, A.T., Jalinous, R., and Freeston, I.L. (1985). Non-invasive magnetic stimulation of
392 human motor cortex. *Lancet Lond. Engl.* *1*, 1106–1107. [https://doi.org/10.1016/s0140-6736\(85\)92413-4](https://doi.org/10.1016/s0140-6736(85)92413-4).
- 394 3. Rothwell, J.C., Thompson, P.D., Day, B.L., Boyd, S., and Marsden, C.D. (1991).
396 Stimulation of the human motor cortex through the scalp. *Exp. Physiol.* *76*, 159–200.
<https://doi.org/10.1113/expphysiol.1991.sp003485>.
4. Lefaucheur, J.-P. (2009). Methods of therapeutic cortical stimulation. *Neurophysiol. Clin. Clin. Neurophysiol.* *39*, 1–14. <https://doi.org/10.1016/j.neucli.2008.11.001>.
5. Lefaucheur, J.-P., Aleman, A., Baeken, C., Benninger, D.H., Brunelin, J., Di Lazzaro, V., Filipović, S.R., Grefkes, C., Hasan, A., Hummel, F.C., et al. (2020). Evidence-based guidelines on the therapeutic use of repetitive transcranial magnetic stimulation (rTMS): An

- 398 update (2014-2018). *Clin. Neurophysiol. Off. J. Int. Fed. Clin. Neurophysiol.* *131*, 474–528.
399 <https://doi.org/10.1016/j.clinph.2019.11.002>.
- 400 6. George, M.S., Wassermann, E.M., Williams, W.A., Callahan, A., Ketter, T.A., Basser, P.,
401 Hallett, M., and Post, R.M. (1995). Daily repetitive transcranial magnetic stimulation (rTMS)
402 improves mood in depression. *Neuroreport* *6*, 1853–1856.
403 <https://doi.org/10.1097/00001756-199510020-00008>.
- 404 7. Pascual-Leone, A., Rubio, B., Pallardó, F., and Catalá, M.D. (1996). Rapid-rate
405 transcranial magnetic stimulation of left dorsolateral prefrontal cortex in drug-resistant
406 depression. *Lancet Lond. Engl.* *348*, 233–237. [https://doi.org/10.1016/s0140-6736\(96\)01219-6](https://doi.org/10.1016/s0140-6736(96)01219-6).
- 408 8. Acevedo, N., Bosanac, P., Pikoos, T., Rossell, S., and Castle, D. (2021). Therapeutic
409 Neurostimulation in Obsessive-Compulsive and Related Disorders: A Systematic Review.
410 *Brain Sci.* *11*, 948. <https://doi.org/10.3390/brainsci11070948>.
- 412 9. Pell, G.S., Roth, Y., and Zangen, A. (2011). Modulation of cortical excitability induced by
413 repetitive transcranial magnetic stimulation: Influence of timing and geometrical
414 parameters and underlying mechanisms. *Prog. Neurobiol.* *93*, 59–98.
415 <https://doi.org/10.1016/j.pneurobio.2010.10.003>.
- 416 10. Suppa, A., Ascii, F., and Guerra, A. (2022). Transcranial magnetic stimulation as a tool to
417 induce and explore plasticity in humans. In *Handbook of Clinical Neurology*, A. Quartarone,
418 M. F. Ghilardi, and F. Boller, eds. (Elsevier), pp. 73–89. <https://doi.org/10.1016/B978-0-12-819410-2.00005-9>.
- 420 11. George, M.S., Lisanby, S.H., Avery, D., McDonald, W.M., Durkalski, V., Pavlicova, M.,
421 Anderson, B., Nahas, Z., Bulow, P., Zarkowski, P., et al. (2010). Daily Left Prefrontal
422 Transcranial Magnetic Stimulation Therapy for Major Depressive Disorder: A Sham-
423 Controlled Randomized Trial. *Arch. Gen. Psychiatry* *67*, 507–516.
424 <https://doi.org/10.1001/archgenpsychiatry.2010.46>.
- 426 12. Mirman, A.M., Corlier, J., Wilson, A.C., Tadayonnejad, R., Marder, K.G., Pleman, C.M.,
427 Krantz, D.E., Wilke, S.A., Levitt, J.G., Ginder, N.D., et al. (2022). Absence of early mood
428 improvement as a robust predictor of rTMS nonresponse in major depressive disorder.
429 *Depress. Anxiety* *39*, 123–133. <https://doi.org/10.1002/da.23237>.
- 430 13. George, M.S., Ketter, T.A., and Post, R.M. (1994). Prefrontal cortex dysfunction in clinical
431 depression. *Depression* *2*, 59–72. <https://doi.org/10.1002/depr.3050020202>.
- 432 14. Fitzgerald, P.B., Laird, A.R., Maller, J., and Daskalakis, Z.J. (2008). A meta-analytic study
433 of changes in brain activation in depression. *Hum. Brain Mapp.* *29*, 683–695.
434 <https://doi.org/10.1002/hbm.20426>.
- 436 15. Elbau, I.G., Lynch, C.J., Downar, J., Vila-Rodriguez, F., Power, J.D., Solomonov, N.,
437 Daskalakis, Z.J., Blumberger, D.M., and Liston, C. (2023). Functional Connectivity
438 Mapping for rTMS Target Selection in Depression. *Am. J. Psychiatry* *180*, 230–240.
439 <https://doi.org/10.1176/appi.ajp.20220306>.
- 440 16. Young, I.M., Taylor, H.M., Nicholas, P.J., Mackenzie, A., Tanglay, O., Dadario, N.B.,
441 Osipowicz, K., Davis, E., Doyen, S., Teo, C., et al. (2023). An agile, data-driven approach
442 for target selection in rTMS therapy for anxiety symptoms: Proof of concept and
443 preliminary data for two novel targets. *Brain Behav.* *13*, e2914.
444 <https://doi.org/10.1002/brb3.2914>.
- 446 17. Brown, K.E., Neva, J.L., Ledwell, N.M., and Boyd, L.A. (2014). Use of transcranial
447 magnetic stimulation in the treatment of selected movement disorders. *Degener. Neurol.*
448 *Neuromuscul. Dis.* *4*, 133–151. <https://doi.org/10.2147/DNND.S70079>.
- 449 18. Vlachos, A., Müller-Dahlhaus, F., Rosskopp, J., Lenz, M., Ziemann, U., and Deller, T.
450 (2012). Repetitive magnetic stimulation induces functional and structural plasticity of
451 excitatory postsynapses in mouse organotypic hippocampal slice cultures. *J. Neurosci. Off.*
452 *J. Soc. Neurosci.* *32*, 17514–17523. <https://doi.org/10.1523/JNEUROSCI.0409-12.2012>.

- 450 19. Lenz, M., Platschek, S., Priesemann, V., Becker, D., Willems, L.M., Ziemann, U., Deller,
452 T., Müller-Dahlhaus, F., Jedlicka, P., and Vlachos, A. (2015). Repetitive magnetic
stimulation induces plasticity of excitatory postsynapses on proximal dendrites of cultured
454 mouse CA1 pyramidal neurons. *Brain Struct. Funct.* 220, 3323–3337.
<https://doi.org/10.1007/s00429-014-0859-9>.
- 456 20. Funke, K., and Benali, A. (2011). Modulation of cortical inhibition by rTMS - findings
458 obtained from animal models. *J. Physiol.* 589, 4423–4435.
<https://doi.org/10.1113/jphysiol.2011.206573>.
- 460 21. Lenz, M., Galanis, C., Müller-Dahlhaus, F., Opitz, A., Wierenga, C.J., Szabó, G., Ziemann,
462 U., Deller, T., Funke, K., and Vlachos, A. (2016). Repetitive magnetic stimulation induces
464 plasticity of inhibitory synapses. *Nat. Commun.* 7, 10020.
<https://doi.org/10.1038/ncomms10020>.
- 466 22. Trippe, J., Mix, A., Aydin-Abidin, S., Funke, K., and Benali, A. (2009). θ burst and
468 conventional low-frequency rTMS differentially affect GABAergic neurotransmission in the
470 rat cortex. *Exp. Brain Res.* 199, 411–421. <https://doi.org/10.1007/s00221-009-1961-8>.
- 472 23. Cole, E.J., Stimpson, K.H., Bentzley, B.S., Gulser, M., Cherian, K., Tischler, C., Nejad, R.,
474 Pankow, H., Choi, E., Aaron, H., et al. (2020). Stanford Accelerated Intelligent
476 Neuromodulation Therapy for Treatment-Resistant Depression. *Am. J. Psychiatry* 177,
716–726. <https://doi.org/10.1176/appi.ajp.2019.19070720>.
- 478 24. Cole, E.J., Phillips, A.L., Bentzley, B.S., Stimpson, K.H., Nejad, R., Barmak, F., Veerapal,
480 C., Khan, N., Cherian, K., Felber, E., et al. (2022). Stanford Neuromodulation Therapy
482 (SNT): A Double-Blind Randomized Controlled Trial. *Am. J. Psychiatry* 179, 132–141.
<https://doi.org/10.1176/appi.ajp.2021.20101429>.
- 484 25. van Rooij, S.J.H., Arulpragasam, A.R., McDonald, W.M., and Philip, N.S. (2024).
486 Accelerated TMS - moving quickly into the future of depression treatment.
488 *Neuropsychopharmacology* 49, 128–137. <https://doi.org/10.1038/s41386-023-01599-z>.
- 490 26. Cohen, D., and Cuffin, B.N. (1991). Developing a More Focal Magnetic Stimulator. Part I:
492 Some Basic Principles. *J. Clin. Neurophysiol.* 8, 102.
- 494 27. Wilson, M.T., Tang, A.D., Iyer, K., McKee, H., Waas, J., and Rodger, J. (2018). The
496 challenges of producing effective small coils for transcranial magnetic stimulation of mice.
498 *Biomed. Phys. Eng. Express* 4, 037002. <https://doi.org/10.1088/2057-1976/aab525>.
- 500 28. Gersner, R., Kravetz, E., Feil, J., Pell, G., and Zangen, A. (2011). Long-Term Effects of
502 Repetitive Transcranial Magnetic Stimulation on Markers for Neuroplasticity: Differential
504 Outcomes in Anesthetized and Awake Animals. *J. Neurosci.* 31, 7521–7526.
<https://doi.org/10.1523/JNEUROSCI.6751-10.2011>.
- 506 29. Tang, A.D., Lowe, A.S., Garrett, A.R., Woodward, R., Bennett, W., Canty, A.J., Garry, M.I.,
508 Hinder, M.R., Summers, J.J., Gersner, R., et al. (2016). Construction and Evaluation of
510 Rodent-Specific rTMS Coils. *Front. Neural Circuits* 10.
<https://doi.org/10.3389/fncir.2016.00047>.
- 512 30. Vahabzadeh-Hagh, A.M., Muller, P.A., Gersner, R., Zangen, A., and Rotenberg, A. (2012).
514 Translational Neuromodulation: Approximating Human Transcranial Magnetic Stimulation
516 Protocols in Rats. *Neuromodulation Technol. Neural Interface* 15, 296–305.
<https://doi.org/10.1111/j.1525-1403.2012.00482.x>.
- 518 31. Rotenberg, A., Muller, P.A., Vahabzadeh-Hagh, A.M., Navarro, X., López-Vales, R.,
520 Pascual-Leone, A., and Jensen, F. (2010). Lateralization of forelimb motor evoked
522 potentials by transcranial magnetic stimulation in rats. *Clin. Neurophysiol.* 121, 104–108.
<https://doi.org/10.1016/j.clinph.2009.09.008>.
- 524 32. Alekseichuk, I., Mantell, K., Shirinpour, S., and Opitz, A. (2019). Comparative modeling of
526 transcranial magnetic and electric stimulation in mouse, monkey, and human. *NeuroImage*
528 194, 136–148. <https://doi.org/10.1016/j.neuroimage.2019.03.044>.
- 530 33. Parthoens, J., Verhaeghe, J., Servaes, S., Miranda, A., Stroobants, S., and Staelens, S.

- 500 (2016). Performance Characterization of an Actively Cooled Repetitive Transcranial
502 Magnetic Stimulation Coil for the Rat. *Neuromodulation Technol. Neural Interface* *19*, 459–
468. <https://doi.org/10.1111/ner.12387>.
34. Meng, Q., Jing, L., Badjo, J.P., Du, X., Hong, E., Yang, Y., Lu, H., and Choa, F.-S. (2018).
504 A novel transcranial magnetic stimulator for focal stimulation of rodent brain. *Brain*
Stimulat. *11*, 663–665. <https://doi.org/10.1016/j.brs.2018.02.018>.
- 506 35. Meng, Q., Nguyen, H., Vrana, A., Baldwin, S., Li, C.Q., Giles, A., Wang, J., Yang, Y., and
508 Lu, H. (2022). A high-density theta burst paradigm enhances the aftereffects of transcranial
magnetic stimulation: Evidence from focal stimulation of rat motor cortex. *Brain Stimulat.*
15, 833–842. <https://doi.org/10.1016/j.brs.2022.05.017>.
- 510 36. Cermak, S., Meng, Q., Peng, K., Baldwin, S., Mejías-Aponte, C.A., Yang, Y., and Lu, H.
512 (2020). Focal transcranial magnetic stimulation in awake rats: enhanced glucose uptake in
deep cortical layers. *J. Neurosci. Methods* *339*, 108709.
<https://doi.org/10.1016/j.jneumeth.2020.108709>.
- 514 37. Bagherzadeh, H., Meng, Q., Deng, Z.-D., Lu, H., Hong, E., Yang, Y., and Choa, F.-S.
516 (2022). Angle-tuned coils: attractive building blocks for TMS with improved depth-spread
performance. *J. Neural Eng.* *19*, 10.1088/1741-2552/ac697c. <https://doi.org/10.1088/1741-2552/ac697c>.
- 518 38. Tennant, K.A., Adkins, D.L., Donlan, N.A., Asay, A.L., Thomas, N., Kleim, J.A., and Jones,
520 T.A. (2011). The Organization of the Forelimb Representation of the C57BL/6 Mouse
Motor Cortex as Defined by Intracortical Microstimulation and Cytoarchitecture. *Cereb.*
Cortex *21*, 865–876. <https://doi.org/10.1093/cercor/bhq159>.
- 522 39. Li, C.-X., and Waters, R.S. (1991). Organization of the Mouse Motor Cortex Studied by
524 Retrograde Tracing and Intracortical Microstimulation (ICMS) Mapping. *Can. J. Neurol. Sci.*
18, 28–38. <https://doi.org/10.1017/S0317167100031267>.
- 526 40. Huang, Y.-Z., Edwards, M.J., Rounis, E., Bhatia, K.P., and Rothwell, J.C. (2005). Theta
burst stimulation of the human motor cortex. *Neuron* *45*, 201–206.
<https://doi.org/10.1016/j.neuron.2004.12.033>.
- 528 41. Raj, K.S., Geoly, A.D., Veerapal, C., Gholmieh, M., Toosi, P., Espil, F.M., Batail, J.-M.,
530 Kratter, I.H., and Williams, N.R. (2024). Pilot study of stanford neuromodulation therapy
(SNT) for bipolar depression. *Brain Stimul. Basic Transl. Clin. Res. Neuromodulation* *17*,
321–323. <https://doi.org/10.1016/j.brs.2024.03.002>.
- 532 42. Suzuki, M., Furihata, R., Konno, C., Kaneita, Y., Ohida, T., and Uchiyama, M. (2018).
534 Stressful events and coping strategies associated with symptoms of depression: A
Japanese general population survey. *J. Affect. Disord.* *238*, 482–488.
<https://doi.org/10.1016/j.jad.2018.06.024>.
- 536 43. Tafet, G.E., and Nemeroff, C.B. (2016). The Links Between Stress and Depression:
538 Psychoneuroendocrinological, Genetic, and Environmental Interactions. *J. Neuropsychiatry*
Clin. Neurosci. *28*, 77–88. <https://doi.org/10.1176/appi.neuropsych.15030053>.
- 540 44. Radley, J.J., Rocher, A.B., Miller, M., Janssen, W.G.M., Liston, C., Hof, P.R., McEwen,
542 B.S., and Morrison, J.H. (2006). Repeated stress induces dendritic spine loss in the rat
medial prefrontal cortex. *Cereb. Cortex N. Y. N 1991* *16*, 313–320.
<https://doi.org/10.1093/cercor/bhi104>.
- 544 45. Radley, J.J., Rocher, A.B., Rodriguez, A., Ehlenberger, D.B., Dammann, M., McEwen,
546 B.S., Morrison, J.H., Wearne, S.L., and Hof, P.R. (2008). REPEATED STRESS ALTERS
DENDRITIC SPINE MORPHOLOGY IN THE RAT MEDIAL PREFRONTAL CORTEX. *J.*
Comp. Neurol. *507*, 1141–1150. <https://doi.org/10.1002/cne.21588>.
- 548 46. Moda-Sava, R.N., Murdock, M.H., Parekh, P.K., Fetcho, R.N., Huang, B.S., Huynh, T.N.,
550 Witztum, J., Shaver, D.C., Rosenthal, D.L., Alway, E.J., et al. (2019). Sustained rescue of
prefrontal circuit dysfunction by antidepressant-induced spine formation. *Science* *364*,
eaat8078. <https://doi.org/10.1126/science.aat8078>.

47. Fetcho, R.N., Parekh, P.K., Chou, J., Kenwood, M., Chalénçon, L., Estrin, D.J., Johnson, M., and Liston, C. (2024). A stress-sensitive frontostriatal circuit supporting effortful reward-seeking behavior. *Neuron* 112, 473-487.e4.
552
554 <https://doi.org/10.1016/j.neuron.2023.10.020>.
48. Orzechowska, A., Zajączkowska, M., Talarowska, M., and Gałęcki, P. (2013). Depression and ways of coping with stress: a preliminary study. *Med. Sci. Monit. Int. Med. J. Exp. Clin. Res.* 19, 1050–1056. <https://doi.org/10.12659/MSM.889778>.
556
49. Li, N., Lee, B., Liu, R.-J., Banasr, M., Dwyer, J.M., Iwata, M., Li, X.-Y., Aghajanian, G., and Duman, R.S. (2010). mTOR-dependent synapse formation underlies the rapid antidepressant effects of NMDA antagonists. *Science* 329, 959–964.
558
560 <https://doi.org/10.1126/science.1190287>.
50. Kwan, A.C., Olson, D.E., Preller, K.H., and Roth, B.L. (2022). The neural basis of psychedelic action. *Nat. Neurosci.* 25, 1407–1419. <https://doi.org/10.1038/s41593-022-01177-4>.
562
564
51. Gourley, S.L., and Taylor, J.R. (2009). Recapitulation and Reversal of a Persistent Depression-like Syndrome in Rodents. *Curr. Protoc. Neurosci.* 49, 9.32.1-9.32.11.
566 <https://doi.org/10.1002/0471142301.ns0932s49>.
52. Marks, W., Fournier, N.M., and Kalynchuk, L.E. (2009). Repeated exposure to corticosterone increases depression-like behavior in two different versions of the forced swim test without altering nonspecific locomotor activity or muscle strength. *Physiol. Behav.* 98, 67–72. <https://doi.org/10.1016/j.physbeh.2009.04.014>.
568
570
53. Wróbel, A., Serefko, A., Poleszak, E., and Rechberger, T. (2016). Fourteen-day administration of corticosterone may induce detrusor overactivity symptoms. *Int. Urogynecology J.* 27, 1713–1721. <https://doi.org/10.1007/s00192-016-3027-3>.
572
574
54. Nollet, M. (2021). Models of Depression: Unpredictable Chronic Mild Stress in Mice. *Curr. Protoc.* 1, e208. <https://doi.org/10.1002/cpz1.208>.
576
55. Rawat, R., Tunc-Ozcan, E., McGuire, T.L., Peng, C.-Y., and Kessler, J.A. (2022). Ketamine activates adult-born immature granule neurons to rapidly alleviate depression-like behaviors in mice. *Nat. Commun.* 13, 2650. <https://doi.org/10.1038/s41467-022-30386-5>.
578
580
56. Gorman, J.M. (1996). Comorbid depression and anxiety spectrum disorders. *Depress. Anxiety* 4, 160–168. [https://doi.org/10.1002/\(SICI\)1520-6394\(1996\)4:4<160::AID-DA2>3.0.CO;2-J](https://doi.org/10.1002/(SICI)1520-6394(1996)4:4<160::AID-DA2>3.0.CO;2-J).
582
57. Tuinstra, D., Percifield, C., Stilwell, K., Plattner, A., Edwards, E., Sanders, W., and Koval, M. (2022). Treatment of anxiety symptoms in patients receiving rTMS for treatment resistant depression. *Psychiatry Res. Commun.* 2, 100014. <https://doi.org/10.1016/j.psychom.2021.100014>.
584
586
58. Stanton, C.H., Holmes, A.J., Chang, S.W.C., and Joormann, J. (2019). From Stress to Anhedonia: Molecular Processes through Functional Circuits. *Trends Neurosci.* 42, 23–42. <https://doi.org/10.1016/j.tins.2018.09.008>.
588
590
59. Prevot, T.D., Misquitta, K.A., Fee, C., Newton, D.F., Chatterjee, D., Nikolova, Y.S., Sibille, E., and Banasr, M. (2019). Residual avoidance: A new, consistent and repeatable readout of chronic stress-induced conflict anxiety reversible by antidepressant treatment. *Neuropharmacology* 153, 98–110. <https://doi.org/10.1016/j.neuropharm.2019.05.005>.
592
594
60. Floris, G., Godar, S.C., Braccagni, G., Piras, I.S., Ravens, A., Zanda, M.T., Huentelman, M.J., and Bortolato, M. (2024). The sinking platform test: a novel paradigm to measure persistence in animal models. *Neuropsychopharmacology* 49, 1373–1382. <https://doi.org/10.1038/s41386-024-01827-0>.
596
598
61. Liu, M.-Y., Yin, C.-Y., Zhu, L.-J., Zhu, X.-H., Xu, C., Luo, C.-X., Chen, H., Zhu, D.-Y., and Zhou, Q.-G. (2018). Sucrose preference test for measurement of stress-induced anhedonia in mice. *Nat. Protoc.* 13, 1686–1698. <https://doi.org/10.1038/s41596-018-0011->
600

- 602 z.
- 604 62. Letkiewicz, A.M., Kottler, H.C., Shankman, S.A., and Cochran, A.L. (2023). Quantifying
606 aberrant approach-avoidance conflict in psychopathology: A review of computational
608 approaches. *Neurosci. Biobehav. Rev.* *147*, 105103.
610 <https://doi.org/10.1016/j.neubiorev.2023.105103>.
- 612 63. Zeidler, Z., Gómez, M.F., Gupta, T.A., Shari, M., Wilke, S.A., and DeNardo, L.A. (2024).
614 Prefrontal dopamine circuits are required for active avoidance learning but not for fear
616 learning. Preprint at bioRxiv, <https://doi.org/10.1101/2024.05.02.592069>
<https://doi.org/10.1101/2024.05.02.592069>.
- 618 64. Russo, S.J., and Nestler, E.J. (2013). The brain reward circuitry in mood disorders. *Nat.*
620 *Rev. Neurosci.* *14*, 609–625. <https://doi.org/10.1038/nrn3381>.
- 622 65. Warden, M.R., Selimbeyoglu, A., Mirzabekov, J.J., Lo, M., Thompson, K.R., Kim, S.-Y.,
624 Adhikari, A., Tye, K.M., Frank, L.M., and Deisseroth, K. (2012). A prefrontal cortex–
626 brainstem neuronal projection that controls response to behavioural challenge. *Nature* *492*,
628 428–432. <https://doi.org/10.1038/nature11617>.
- 630 66. Hare, B.D., Shinohara, R., Liu, R.J., Pothula, S., DiLeone, R.J., and Duman, R.S. (2019).
632 Optogenetic stimulation of medial prefrontal cortex *Drd1* neurons produces rapid and long-
634 lasting antidepressant effects. *Nat. Commun.* *10*, 223. <https://doi.org/10.1038/s41467-018-08168-9>.
- 636 67. Shrestha, P., Mousa, A., and Heintz, N. (2015). Layer 2/3 pyramidal cells in the medial
638 prefrontal cortex moderate stress induced depressive behaviors. *eLife* *4*, e08752.
640 <https://doi.org/10.7554/eLife.08752>.
- 642 68. Cai, Y., Ge, J., and Pan, Z.Z. (2024). The projection from dorsal medial prefrontal cortex to
644 basolateral amygdala promotes behaviors of negative emotion in rats. *Front. Neurosci.* *18*.
646 <https://doi.org/10.3389/fnins.2024.1331864>.
- 648 69. Johnson, S.B., Lingg, R.T., Skog, T.D., Hinz, D.C., Romig-Martin, S.A., Viau, V.,
650 Narayanan, N.S., and Radley, J.J. (2022). Activity in a prefrontal-periaqueductal gray
652 circuit overcomes behavioral and endocrine features of the passive coping stress
response. *Proc. Natl. Acad. Sci. U. S. A.* *119*, e2210783119.
<https://doi.org/10.1073/pnas.2210783119>.
- 654 70. Wilke, S.A., Lavi, K., Byeon, S., Donohue, K.C., and Sohal, V.S. (2022). Convergence of
656 Clinically Relevant Manipulations on Dopamine-Regulated Prefrontal Activity Underlying
658 Stress Coping Responses. *Biol. Psychiatry* *91*, 810–820.
<https://doi.org/10.1016/j.biopsych.2021.11.008>.
- 660 71. Gongwer, M.W., Klune, C.B., Couto, J., Jin, B., Enos, A.S., Chen, R., Friedmann, D., and
662 DeNardo, L.A. (2023). Brain-wide projections and differential encoding of prefrontal
664 neuronal classes underlying learned and innate threat avoidance. *J. Neurosci.*
<https://doi.org/10.1523/JNEUROSCI.0697-23.2023>.
- 666 72. Gao, L., Liu, S., Gou, L., Hu, Y., Liu, Y., Deng, L., Ma, D., Wang, H., Yang, Q., Chen, Z., et
668 al. (2022). Single-neuron projectome of mouse prefrontal cortex. *Nat. Neurosci.* *25*, 515–
670 529. <https://doi.org/10.1038/s41593-022-01041-5>.
- 672 73. Gerfen, C.R., Economo, M.N., and Chandrashekar, J. (2018). Long distance projections of
674 cortical pyramidal neurons. *J. Neurosci. Res.* *96*, 1467–1475.
<https://doi.org/10.1002/jnr.23978>.
- 676 74. Harris, K.D., and Shepherd, G.M.G. (2015). The neocortical circuit: themes and variations.
678 *Nat. Neurosci.* *18*, 170–181. <https://doi.org/10.1038/nn.3917>.
- 680 75. Anastasiades, P.G., and Carter, A.G. (2021). Circuit organization of the rodent medial
682 prefrontal cortex. *Trends Neurosci.* *44*, 550–563. <https://doi.org/10.1016/j.tins.2021.03.006>.
- 684 76. Anastasiades, P.G., Collins, D.P., and Carter, A.G. (2021). Mediodorsal and Ventromedial
686 Thalamus Engage Distinct L1 Circuits in the Prefrontal Cortex. *Neuron* *109*, 314–330.e4.
<https://doi.org/10.1016/j.neuron.2020.10.031>.

- 654 77. Anastasiades, P.G., Marlin, J.J., and Carter, A.G. (2018). Cell-Type Specificity of Callosally
Evoked Excitation and Feedforward Inhibition in the Prefrontal Cortex. *Cell Rep.* 22, 679–
692. <https://doi.org/10.1016/j.celrep.2017.12.073>.
- 656 78. Collins, D.P., Anastasiades, P.G., Marlin, J.J., and Carter, A.G. (2018). Reciprocal Circuits
Linking the Prefrontal Cortex with Dorsal and Ventral Thalamic Nuclei. *Neuron* 98, 366–
658 379.e4. <https://doi.org/10.1016/j.neuron.2018.03.024>.
- 660 79. Yao, Z., van Velthoven, C.T.J., Kunst, M., Zhang, M., McMillen, D., Lee, C., Jung, W.,
Goldy, J., Abdelhak, A., Aitken, M., et al. (2023). A high-resolution transcriptomic and
spatial atlas of cell types in the whole mouse brain. *Nature* 624, 317–332.
662 <https://doi.org/10.1038/s41586-023-06812-z>.
- 664 80. Shepherd, G.M.G. (2013). Corticostriatal connectivity and its role in disease. *Nat. Rev.*
Neurosci. 14, 278–291. <https://doi.org/10.1038/nrn3469>.
- 666 81. Pastor, V., and Medina, J.H. (2021). Medial prefrontal cortical control of reward- and
aversion-based behavioral output: Bottom-up modulation. *Eur. J. Neurosci.* 53, 3039–
3062. <https://doi.org/10.1111/ejn.15168>.
- 668 82. Coley, A.A., Padilla-Coreano, N., Patel, R., and Tye, K.M. (2021). Chapter Seven -
Valence processing in the PFC: Reconciling circuit-level and systems-level views. In
670 *International Review of Neurobiology What does Medial Frontal Cortex Signal During*
Behavior? Insights from Behavioral Neurophysiology., A. T. Brockett, L. M. Amarante, M.
672 Laubach, and M. R. Roesch, eds. (Academic Press), pp. 171–212.
<https://doi.org/10.1016/bs.irn.2020.12.002>.
- 674 83. Parekh, P.K., Johnson, S.B., and Liston, C. (2022). Synaptic mechanisms regulating mood
state transitions in depression. *Annu. Rev. Neurosci.* 45, 581–601.
676 <https://doi.org/10.1146/annurev-neuro-110920-040422>.
- 678 84. Kang, H.J., Voleti, B., Hajszan, T., Rajkowska, G., Stockmeier, C.A., Licznarski, P.,
Lepack, A., Majik, M.S., Jeong, L.S., Banasr, M., et al. (2012). Decreased expression of
synapse-related genes and loss of synapses in major depressive disorder. *Nat. Med.* 18,
680 1413–1417. <https://doi.org/10.1038/nm.2886>.
- 682 85. Dias-Ferreira, E., Sousa, J.C., Melo, I., Morgado, P., Mesquita, A.R., Cerqueira, J.J.,
Costa, R.M., and Sousa, N. (2009). Chronic stress causes frontostriatal reorganization and
affects decision-making. *Science* 325, 621–625. <https://doi.org/10.1126/science.1171203>.
- 684 86. Liston, C., Miller, M.M., Goldwater, D.S., Radley, J.J., Rocher, A.B., Hof, P.R., Morrison,
J.H., and McEwen, B.S. (2006). Stress-induced alterations in prefrontal cortical dendritic
686 morphology predict selective impairments in perceptual attentional set-shifting. *J. Neurosci.*
Off. J. Soc. Neurosci. 26, 7870–7874. <https://doi.org/10.1523/JNEUROSCI.1184-06.2006>.
- 688 87. Bessa, J.M., Ferreira, D., Melo, I., Marques, F., Cerqueira, J.J., Palha, J.A., Almeida,
O.F.X., and Sousa, N. (2009). The mood-improving actions of antidepressants do not
690 depend on neurogenesis but are associated with neuronal remodeling. *Mol. Psychiatry* 14,
764–773, 739. <https://doi.org/10.1038/mp.2008.119>.
- 692 88. Hesselgrave, N., Troppoli, T.A., Wulff, A.B., Cole, A.B., and Thompson, S.M. (2021).
Harnessing psilocybin: antidepressant-like behavioral and synaptic actions of psilocybin
694 are independent of 5-HT_{2R} activation in mice. *Proc. Natl. Acad. Sci. U. S. A.* 118,
e2022489118. <https://doi.org/10.1073/pnas.2022489118>.
- 696 89. Shao, L.-X., Liao, C., Gregg, I., Davoudian, P.A., Savalia, N.K., Delagarza, K., and Kwan,
A.C. (2021). Psilocybin induces rapid and persistent growth of dendritic spines in frontal
698 cortex in vivo. *Neuron* 109, 2535-2544.e4. <https://doi.org/10.1016/j.neuron.2021.06.008>.
- 700 90. Huang, Y.-Z., Chen, R.-S., Rothwell, J.C., and Wen, H.-Y. (2007). The after-effect of
human theta burst stimulation is NMDA receptor dependent. *Clin. Neurophysiol. Off. J. Int.*
Fed. Clin. Neurophysiol. 118, 1028–1032. <https://doi.org/10.1016/j.clinph.2007.01.021>.
- 702 91. Teo, J.T.H., Swayne, O.B., and Rothwell, J.C. (2007). Further evidence for NMDA-
dependence of the after-effects of human theta burst stimulation. *Clin. Neurophysiol. Off. J.*

- 704 Int. Fed. Clin. Neurophysiol. *118*, 1649–1651. <https://doi.org/10.1016/j.clinph.2007.04.010>.
- 706 92. Selby, B., MacMaster, F.P., Kirton, A., and McGirr, A. (2019). d-cycloserine blunts motor
708 cortex facilitation after intermittent theta burst transcranial magnetic stimulation: A double-
710 blind randomized placebo-controlled crossover study. *Brain Stimulat.* *12*, 1063–1065.
712 <https://doi.org/10.1016/j.brs.2019.03.026>.
- 714 93. Brown, J.C., Yuan, S., DeVries, W.H., Armstrong, N.M., Korte, J.E., Sahlem, G.L.,
716 Carpenter, L.L., and George, M.S. (2021). NMDA-Receptor Agonist Reveals LTP-like
718 Properties of 10-Hz rTMS in the Human Motor Cortex. *Brain Stimulat.* *14*, 619–621.
720 <https://doi.org/10.1016/j.brs.2021.03.016>.
- 722 94. Thickbroom, G.W. (2007). Transcranial magnetic stimulation and synaptic plasticity:
724 experimental framework and human models. *Exp. Brain Res.* *180*, 583–593.
726 <https://doi.org/10.1007/s00221-007-0991-3>.
- 728 95. Ridding, M.C., and Ziemann, U. (2010). Determinants of the induction of cortical plasticity
730 by non-invasive brain stimulation in healthy subjects. *J. Physiol.* *588*, 2291–2304.
732 <https://doi.org/10.1113/jphysiol.2010.190314>.
- 734 96. Veldman, M.B., Park, C.S., Eyermann, C.M., Zhang, J.Y., Zuniga-Sanchez, E., Hirano,
736 A.A., Daigle, T.L., Foster, N.N., Zhu, M., Langfelder, P., et al. (2020). Brainwide Genetic
738 Sparse Cell Labeling to Illuminate the Morphology of Neurons and Glia with Cre-
740 Dependent MORF Mice. *Neuron* *108*, 111-127.e6.
742 <https://doi.org/10.1016/j.neuron.2020.07.019>.
- 744 97. Little, J.P., and Carter, A.G. (2012). Subcellular synaptic connectivity of layer 2 pyramidal
746 neurons in the medial prefrontal cortex. *J. Neurosci. Off. J. Soc. Neurosci.* *32*, 12808–
748 12819. <https://doi.org/10.1523/JNEUROSCI.1616-12.2012>.
- 750 98. Armbruster, B.N., Li, X., Pausch, M.H., Herlitze, S., and Roth, B.L. (2007). Evolving the
752 lock to fit the key to create a family of G protein-coupled receptors potently activated by an
754 inert ligand. *Proc. Natl. Acad. Sci.* *104*, 5163–5168.
<https://doi.org/10.1073/pnas.0700293104>.
99. Amer, A., and Martin, J.H. (2022). Repeated motor cortex theta-burst stimulation produces
persistent strengthening of corticospinal motor output and durable spinal cord structural
changes in the rat. *Brain Stimulat.* *15*, 1013–1022.
<https://doi.org/10.1016/j.brs.2022.07.005>.
100. Lee, C.-W., Chu, M.-C., Wu, H.-F., Chung, Y.-J., Hsieh, T.-H., Chang, C.-Y., Lin, Y.-C., Lu,
T.-Y., Chang, C.-H., Chi, H., et al. (2023). Different synaptic mechanisms of intermittent
and continuous theta-burst stimulations in a severe foot-shock induced and treatment-
resistant depression in a rat model. *Exp. Neurol.* *362*, 114338.
<https://doi.org/10.1016/j.expneurol.2023.114338>.
101. Tokay, T., Holl, N., Kirschstein, T., Zschorlich, V., and Köhling, R. (2009). High-frequency
magnetic stimulation induces long-term potentiation in rat hippocampal slices. *Neurosci.*
Lett. *461*, 150–154. <https://doi.org/10.1016/j.neulet.2009.06.032>.
102. Benali, A., Trippe, J., Weiler, E., Mix, A., Petrasch-Parwez, E., Girzalsky, W., Eysel, U.T.,
Erdmann, R., and Funke, K. (2011). Theta-Burst Transcranial Magnetic Stimulation Alters
Cortical Inhibition. *J. Neurosci.* *31*, 1193–1203. <https://doi.org/10.1523/JNEUROSCI.1379-10.2011>.
103. Murphy, S.C., Palmer, L.M., Nyffeler, T., Müri, R.M., and Larkum, M.E. (2016).
Transcranial magnetic stimulation (TMS) inhibits cortical dendrites. *eLife* *5*, e13598.
<https://doi.org/10.7554/eLife.13598>.
104. Anastasiades, P.G., Boada, C., and Carter, A.G. (2019). Cell-Type-Specific D1 Dopamine
Receptor Modulation of Projection Neurons and Interneurons in the Prefrontal Cortex.
Cereb. Cortex *29*, 3224–3242. <https://doi.org/10.1093/cercor/bhy299>.
105. Johnson, S.B., Rocks, D., Chalencón, L., Akgul, G., Elbau, I., Estrin, D., Johnson, K.,
Zhang, R., Lenz, A., Mikofsky, R., et al. Fronto-insular circuit mechanisms of accelerated

- intermittent theta burst stimulation. Co-submitted with this report.
- 756 106. Chen, T., Cheng, L., Ma, J., Yuan, J., Pi, C., Xiong, L., Chen, J., Liu, H., Tang, J., Zhong,
758 Y., et al. (2023). Molecular mechanisms of rapid-acting antidepressants: New perspectives
for developing antidepressants. *Pharmacol. Res.* *194*, 106837.
<https://doi.org/10.1016/j.phrs.2023.106837>.
- 760 107. Krystal, J.H., Kavalali, E.T., and Monteggia, L.M. (2024). Ketamine and rapid
762 antidepressant action: new treatments and novel synaptic signaling mechanisms.
Neuropsychopharmacology *49*, 41–50. <https://doi.org/10.1038/s41386-023-01629-w>.
- 764 108. Koenigs, M., and Grafman, J. (2009). The functional neuroanatomy of depression: distinct
roles for ventromedial and dorsolateral prefrontal cortex. *Behav. Brain Res.* *201*, 239–243.
<https://doi.org/10.1016/j.bbr.2009.03.004>.
- 766 109. Zhao, M.-Z., Song, X.-S., and Ma, J.-S. (2021). Gene × environment interaction in major
768 depressive disorder. *World J. Clin. Cases* *9*, 9368–9375.
<https://doi.org/10.12998/wjcc.v9.i31.9368>.
- 770 110. Wilke, S.A., Johnson, C.L., Corlier, J., Marder, K.G., Wilson, A.C., Pleman, C.M., and
Leuchter, A.F. (2022). Psychostimulant use and clinical outcome of repetitive transcranial
772 magnetic stimulation treatment of major depressive disorder. *Depress. Anxiety* *39*, 397–
406. <https://doi.org/10.1002/da.23255>.
- 774 111. Hunter, A.M., Minzenberg, M.J., Cook, I.A., Krantz, D.E., Levitt, J.G., Rotstein, N.M.,
Chawla, S.A., and Leuchter, A.F. (2019). Concomitant medication use and clinical outcome
776 of repetitive Transcranial Magnetic Stimulation (rTMS) treatment of Major Depressive
Disorder. *Brain Behav.* *9*, e01275. <https://doi.org/10.1002/brb3.1275>.
- 778 112. Cole, E., O’Sullivan, S.J., Tik, M., and Williams, N.R. (2024). Accelerated Theta Burst
Stimulation: Safety, Efficacy, and Future Advancements. *Biol. Psychiatry* *95*, 523–535.
<https://doi.org/10.1016/j.biopsych.2023.12.004>.
- 780 113. Nandi, A., Virmani, G., Barve, A., and Marathe, S. (2021). DBscorer: An Open-Source
782 Software for Automated Accurate Analysis of Rodent Behavior in Forced Swim Test and
Tail Suspension Test. *eNeuro* *8*, ENEURO.0305-21.2021.
<https://doi.org/10.1523/ENEURO.0305-21.2021>.
- 784 114. Mathis, A., Mamidanna, P., Cury, K.M., Abe, T., Murthy, V.N., Mathis, M.W., and Bethge,
M. (2018). DeepLabCut: markerless pose estimation of user-defined body parts with deep
786 learning. *Nat. Neurosci.* *21*, 1281–1289. <https://doi.org/10.1038/s41593-018-0209-y>.
- 788 115. Gabriel, C.J., Zeidler, Z., Jin, B., Guo, C., Goodpaster, C.M., Kashay, A.Q., Wu, A.,
Delaney, M., Cheung, J., DiFazio, L.E., et al. (2022). BehaviorDEPOT is a simple, flexible
790 tool for automated behavioral detection based on markerless pose tracking. *eLife* *11*,
e74314. <https://doi.org/10.7554/eLife.74314>.
- 792 116. Schneider, C.A., Rasband, W.S., and Eliceiri, K.W. (2012). NIH Image to ImageJ: 25 years
of image analysis. *Nat. Methods* *9*, 671–675. <https://doi.org/10.1038/nmeth.2089>.
- 794 117. Arshadi, C., Günther, U., Eddison, M., Harrington, K.I.S., and Ferreira, T.A. (2021). SNT: a
unifying toolbox for quantification of neuronal anatomy. *Nat. Methods* *18*, 374–377.
<https://doi.org/10.1038/s41592-021-01105-7>.

796

Acknowledgements

798 We thank Conor Liston, Shane Johnson, Joshua Barry, Carlos Cepeda, Michael Levine, Liquan
Luo and Baljit Khakh for helpful discussions while designing and planning experiments and helpful
800 comments on the manuscript. We also thank the UCLA Eli and Edythe Broad Stem Cell Research
Center (BSCRC) microscopy core for access to imaging facilities.

802

Funding:

804 National Institutes of Health grant R21MH133212 (SAW, LAD)
National Institutes of Health grant R01MH131858 (SAW)
National Institutes of Health grant R01MH137461 (LAD, SAW)

806 National Institutes of Health grant F30MH134633 (MWG)
National Institutes of Health grant T32GM008042 (MWG)
808 National Institutes of Health grant T32NS048004 (MWG)
Whitehall Research Grant (SAW)
810 Vallee Scholars Award (LAD)

Author contributions:

812 Conceptualization: MWG, AFL, LAD, SAW
Methodology: MWG, ASE, AQ, AQK, GAW, YY, HL, AFL, LAD, SAW
814 Investigation: MWG, AQ, ASE, SARM, CBK, MS, OHW, AH, JPR, HL, LAD, SAW
Visualization: MWG
816 Funding acquisition: MWG, AFL, LAD, SAW
Resources: AFL, LAD, SAW
818 Project administration: MWG, LAD, SAW
Supervision: MWG, AFL, LAD, SAW
820 Writing – original draft: MWG
Writing – review & editing: MWG, HL, AFL, LAD, SAW

822 **Declaration of interests:** The authors declare no competing interests.

824 **Data and materials availability:** All data are available in the main text or the supplementary
826 materials.

828 **Supplementary Materials**

830 Document S1: Figs. S1 to S7 and Table S1

832 **STAR Methods**

834 **EXPERIMENTAL MODEL**

836 Male and female C57BL/6 (Jackson Laboratories #000664 or #005304) or MORF3 mice (Jackson
Laboratories #035403) at least 8 weeks of age were used for all experiments. Mice were
838 maintained on a 12-hour light cycle (lights on 7am-7pm) in a temperature- and humidity-controlled
animal facility. All animal procedures were approved by the University of California, Los Angeles
Chancellor's Animal Research Committee.

840 **METHOD DETAILS**

842 **Surgery**

844 Mice were anesthetized with 3% isoflurane until loss of righting reflex and transferred to a
stereotaxic surgical setup, where anesthesia was maintained with 1-2% isoflurane. The scalp was
846 cleaned with three alternating swabs of betadine and 70% ethanol. 2% Lidocaine was injected
under the scalp as a local anesthetic. A small incision was made in the scalp. For viral injections,
848 a small hole was drilled above the injection target and a hamilton syringe loaded with virus was
lowered to the correct stereotaxic coordinate. Virus was pressure injected at 100nL/minute, and
following completion of the injection the syringe was left in place for 7 minutes and then slowly
850 removed from the skull. Coordinates used for injections were as follows, in mm relative to bregma:
dmPFC: AP 1.45, ML \pm 0.35, DV -1.85; PAG: AP -4.0, ML -0.45, DV -3.0; CLA/Al: AP 1.3, ML -
852 3.25, DV -4.2.

854 While animals were on the stereotaxic rig, we used stereotaxic coordinates to mark the location
for targeting of the TMS coil hotspot. For motor response experiments, a small marker dot was
856 placed above the approximate hindlimb region of the motor cortex using stereotaxic coordinates

858 (AP -1.0, ML +1.5) to use for alignment of the magnet. For dmPFC stimulation and behavioral
860 experiments in Figures 1, 5, and S2-4, the dot was placed at AP 1.45mm, ML 0mm (on the
862 midline) to promote bilateral stimulation. For unilateral fiber photometry and dendritic spine
864 experiments in Figures 2-4, and S6, the dot was placed at AP 1.45mm, ML -0.35mm to stimulate
866 above the tip of the fiber optic cannula.

868 All mice were also implanted with skull bars to allow head fixation during sham or TMS treatment.
870 To do so, muscles on the posterior region of the skull were carefully removed with scissors and a
864 scalpel blade to reveal the skull surface. Light scoring of the skull was performed with a drill, and
866 the area was cleaned with ethanol. A 3D-printed plastic skull bar was then positioned posterior to
868 the skull and cemented in place with metabond (Patterson Dental Company, 5533559, 5533492,
870 S371). Care was taken to avoid buildup of metabond near the site of stimulation. Mice were pre-
and then post-operatively treated with subcutaneous injections of carprofen (50mg/kg) daily for
three days following surgery.

872 For fiber photometry experiments, skin and muscle tissue behind the eye was carefully removed
874 on the side of the skull directly lateral to the target location. A drill was used to clear away bone
876 on the side of the skull, and a 4mm long 400nm optic fiber was slowly inserted through this hole
878 from the lateral direction until it reached the coordinate for dmPFC. Tissue surrounding the fiber
insertion site was dried using compressed air. The fiber was then cemented in place with
metabond followed by installation of a skull bar as above.

878 **Chronic Stress**

880 *Chronic corticosterone administration*

882 Corticosterone (Sigma) was dissolved in 100% ethanol at 10mg/mL, and this was diluted with
884 drinking water from the animal facility to achieve a final concentration of 0.1mg/mL. Mice received
this solution in their home cages in place of normal water for 14 days. Control animals received
normal drinking water, consistent with previous studies⁴⁶.

886 *Unpredictable Chronic Mild Stress*

888 Mice were exposed to two stressors daily for 21 days. Stressors included restraint stress (1-2hr),
890 removal of bedding (2-4hr), ¼ inch of lukewarm water in place of bedding (1-2hr), wet bedding
(1-2hr), tilted cage (2-4hr), rapid air flow in cage (10min), light cycle disturbance (overnight), and
food/water restriction (overnight). Stressors were randomized, and the same stressor was never
presented on two consecutive days⁵⁵.

892 **Behavioral Experiments**

894 *Open Field Test & Elevated Zero Maze*

896 Mice were gently placed in the corner of an open field arena (50x50cm) facing the wall of the
arena. Mice were allowed to explore the arena for 10 minutes while their behavior was recorded
898 with an overhead camera. Mice were then removed from the arena, briefly placed in their home
cage, and then placed at the entry to the closed arm of the EZM. Mice were allowed to explore
the EZM for 10 minutes while their behavior was recorded with an overhead camera. Mice were
900 then returned to their home cage. The OFT and EZM were cleaned with 70% ethanol between
902 each mouse. Time spent in specific zones for each assay was quantified using Biobserve Viewer
software.

904 *Forced swim test*

906 2-liter glass beakers were filled with 25-26°C water and placed against a white background in a
dimly lit room. Mice were gently lowered into the water and their behavior recorded during a 6-
minute window from the side of the beaker. Mice were then removed from the beakers, dried, and

908 placed back in their home cage. Water was changed between each animal. Immobility during the
910 last 4 minutes of the assay was quantified using DBscorer¹¹³, which classifies struggling behavior
912 by calculating the change in the area of the frame taken up by the mouse across time. To ensure
914 consistent baseline levels of immobility in mice undergoing FST both before and after aiTBS
(Figures S1 and 5), only mice with more than 56.5% immobility on the pretest were used for
subsequent aiTBS or sham treatment. This was equivalent to 1 standard deviation below the
mean immobility of all stress mice in Figure 1E.

916 *Sucrose preference test*

918 Mice were placed in individual chambers (25cm L x 10cm W x 12.5 cm H) with two glass drinking
920 bottles (Bio-Serv #9019/9015) suspended on one short end of the chamber⁶¹. Mice were water
922 deprived for 20 hours before each habituation and test session. Mice were first habituated to the
924 setup for 4 hours with both bottles filled with normal drinking water. Mice were then placed back
926 in the chamber for another 4 hour habituation session, this time with 1% sucrose in one of the
928 bottles. The following day the testing session began. Mice were given free choice between normal
930 drinking water and 1% sucrose in water for 4 hours. The position of the bottles were switched
932 halfway through to eliminate effects of a potential side preference. Bottles were weighed before
934 and after the 4 hour session, and sucrose preference was calculated as (grams sucrose solution
consumed) / (total liquid consumed) x 100. 3 test sessions were run before CORT administration,
and the average sucrose preference across these sessions was considered the baseline sucrose
preference. For these animals, CORT administration was extended to 18 days to account for the
potential loss of stress effects once the CORT was removed for water deprivation. Following
CORT, mice were water deprived for one day and another habituation session was performed
with 1% sucrose in one of the bottles, followed by a test session one day later. Mice were treated
with aiTBS or sham the following day. One day after aiTBS or sham treatment, mice were given
another habituation session with 1% sucrose in one of the bottles, followed by a final test session
the next day.

936 *Sinking platform test*

938 An abbreviated version of the sinking platform test⁶⁰ was performed to allow the rapid assessment
940 of persistence behavior shortly after the administration of CORT and subsequent aiTBS
942 treatment. A 32-gallon plastic container 22" in diameter (Brute H-1045) was filled with
944 approximately 10 inches of 32°C water. A custom-built platform 3.35"x4.8" was positioned level
946 with the surface of the water in the locations described in Figure S3D. Locations were varied
948 around the tank, with some located in the center of the tank. On the first day, mice were first
950 exposed to four escape trials, in which climbing the platform resulted in removal from the tank.
952 The same day, a progressive ratio was introduced consisting of an increasing number of failure
954 trials prior to the final escape trial. A failure trial consisted of sinking the platform and repositioning
it after the mouse climbed it, requiring the mouse to swim to the new location. The second day,
two additional training sessions were performed with 4 and 7 failure trials before the escape trial,
respectively. Latency per platform during training was calculated as the total time swimming prior
to climbing the final platform divided by the number of platforms climbed. After these sessions,
the same day, mice were subjected to a test session consisting of exclusively failure trials. The
total number of platforms climbed within 5 minutes was reported for each mouse. Mice were
treated with TMS the following day, and the day 2 protocol was repeated, with two training
sessions followed by a final test session.

954 *Approach-avoidance conflict assay*

956 Mice were food deprived for 4 days prior to the beginning of habituation, receiving free food
958 access for 1 hour per day. Behavior was performed in an operant chamber with a shock floor
(Lafayette Instruments). One quarter of the floor was covered by a plexiglass platform, and in the

960 opposite corner from this platform was a reward pump. The reward pump, fitted with an IR sensor,
962 was set to deliver rewards following head entry at a randomized variable interval schedule
964 averaging 30 seconds per interval, regardless of tone presentation, as previously described⁶³.
966 Mice were habituated to the setup and reward delivery during the final two days of CORT
968 administration to allow for the immediate start of training following aiTBS or sham treatment. The
970 day after treatment, mice received 3 baseline tones with no shock followed by 9 tones which co-
972 terminated with a 2-second mild foot shock (0.13mA). Tones were 4kHz, 70dB, and 30 seconds
in length and were separated by randomized intervals between 80 and 150 seconds. Reward
delivery continued on the variable interval schedule regardless of tone presentation. On the
second day of training, mice received 9 additional tone-shock pairings. On the retrieval day, three
tones were presented without foot shocks. Videos of behavior were obtained using a Point Gray
Chameleon3 camera (Teledyne FLIR). Point-tracking was performed in DeepLabCut¹¹⁴, and
behavior was analyzed using BehaviorDEPOT¹¹⁵. Retrieval videos for two mice (one sham, one
aiTBS) were irreversibly corrupted due to technical difficulties and were not able to be analyzed.

974 **Transcranial Magnetic Stimulation**

976 The rodent TMS coil was assembled as previously described and validated³⁴⁻³⁶. It was connected
978 to a MagStim Rapid² Plus1 stimulator, which was used to power the coil and deliver clinical
980 stimulation protocols. To prevent overheating of the magnet during chronic, high-frequency
982 stimulation, sheets of copper were placed directly against the four long sides of the coil housing,
984 and ¼ inch copper tubing was wrapped around the magnet as shown in Figure 1A. This setup
was designed to optimize heat transfer between the liquid in the copper tubing and the epoxy-
coated coil. An aquarium pump was submerged in a solution of 30% CaCl₂ in water maintained
at -40°C and was used to pump this solution through the copper tubing beginning at the start of
the stimulation session. This maintained the surface of the magnet at approximately room
temperature for the duration of a stimulation session.

986 For motor response measurements, awake mice were scruffed in a way that largely immobilized
988 their limbs, and the hotspot of the magnet was positioned over the marked coordinate. Fine
990 adjustments in head position were made until reliable left hindlimb movement was obtained with
992 single pulses. The magnet intensity was then adjusted to find the minimum threshold at which
50% of pulses resulted in motor responses, which is how motor threshold is assessed in humans.
Across five mice, we estimated the motor threshold to be between 50 and 55% of the maximum
stimulator output.

994 For chronic treatment, mice were head-fixed on a running wheel by clamping surgical hemostats
996 onto their skull bars and gently placing these hemostats into a custom 3D-printed hemostat
998 holder. Mice were habituated to head fixation for at least two days prior to treatment. Prior to each
stimulation session, the stereotaxic marker dot indicating the position of dmPFC was aligned to a
dot indicating the focal 'hotspot' of the TMS coil using a fine 3-axis manipulator. The coil was then
lowered such that the epoxy coating at the 'hotspot' of the magnet pressed directly against the
1000 mouse's skull.

1002 The TMS coil produces an audible clicking noise and slight vibrations during stimulation. To
1004 ensure sham-treated animals had an identical experience to experimental animals, with the
1006 absence of magnetic stimulation, sham mice were always run simultaneously on an identical head
1008 fixation setup directly adjacent to the setup for TMS-treated animals (Fig. S1). This ensured nearly
identical auditory stimuli between groups. In addition, the lid of a 50mL conical tube, which has a
texture similar to the epoxy coating of the real magnet, was pressed directly against the head of
the sham mouse. To account for mechanical sensations during stimulation, the heavy cable

1010 connecting the TMS coil to the stimulator was draped over the sham coil to produce identically-timed vibrations which were transmitted through the sham coil.

1012 Accelerated iTBS was performed using clinically identical stimulation parameters as previously
described^{23,24,41}. Ten 50Hz bursts of 3 pulses, separated by 200ms intervals, were delivered within
1014 a two second window. We refer to this as a 'train'. Trains were delivered every 10 seconds for a
total of 60 trains across a 10-minute stimulation session. 10 sessions were delivered throughout
1016 the treatment day, with a session occurring once per hour. The stimulation intensity was
maintained at 42% of the maximum stimulator output, in line with clinical iTBS, which is typically
1018 delivered at a power between 80 and 90% of the motor threshold. Mice were returned to their
home cage between stimulation sessions.

1020

Fiber Photometry

1022 To record neural activity in IT and PT neurons, 200nL of AAVrg-Ef1a-mCherry-IRES-Cre
(Addgene #55632, 2.2×10^{13} vg/mL) was injected in either right dmPFC or left PAG, respectively.
1024 400nL of AAV1-Syn-FLEX-jGCaMP7f (Addgene #104492, 2.1×10^{13} vg/mL) was then injected into
left dmPFC. Viruses were injected at least 4 weeks prior to the start of recordings. Fiber
1026 photometry signals were recorded using a Tucker-Davis Technologies (TDT) RZ10x processor in
combination with the TDT Synapse software. The 465nm channel representing calcium-driven
1028 changes in GCaMP fluorescence was recorded simultaneously with a 405nm isosbestic channel,
which does not fluctuate with calcium activity. Prior to recording, the light output of each channel
1030 for each mouse was adjusted to a signal of approximately 80mV.

1032 *Recording during rTMS*

To control for auditory-driven neural activity not directly linked to magnetic stimulation, the sound
1034 of the magnet was recorded and played constantly through computer speakers for the duration of
combined TMS and fiber photometry recording. Recordings during iTBS treatment in Figure 2E
1036 were limited to the first session of the day to prevent the constant auditory noise from affecting
behavioral outcomes the following day. A TTL signal connecting the stimulator to the fiber
1038 photometry system allowed alignment of the stimulation and the photometry signal.

1040 *Pavlovian stimuli*

Beginning two days prior to TMS treatment, fiber photometry mice were head-fixed and underwent
1042 pavlovian condition for aversive and rewarding stimuli. Aversive stimuli consisted of a 5-second
7kHz tone at approximately 75dB co-terminating with a 0.5-second air puff. The air puff spout was
1044 positioned approximately 7mm from the eye. Rewarding stimuli consisted of a 5-second 2.9kHz
tone at approximately 75dB co-terminating with a 0.5-second delivery of 25% sweetened
1046 condensed milk via a peristaltic pump. The reward spout was positioned directly in the mouse's
mouth to ensure reward delivery occurred at the exact same time for each stimulus and to
1048 guarantee the mouse received a reward on each trial. On the first day of conditioning, mice
received 6 rewarding stimuli followed by 6 additional rewarding stimuli randomly interspersed with
1050 6 aversive stimuli. On the second day of conditioning, mice received 6 stimuli of each type,
randomly interspersed. Stimuli were separated by a randomized interval between 30 and 60
1052 seconds each. The day after TMS treatment, mice received 6 stimuli of each type, randomly
interspersed, while photometry signals were recorded. Tones, air puffs and rewards were aligned
1054 with fiber photometry signals via TTL pulses delivered to the fiber photometry system.

1056 *Tail suspension test and Open Field Test*

Because FST was not compatible with the lateral fiber optic implant without risking animal safety,
1058 we instead used the tail suspension test to record neural activity during struggling behavior. A
small plastic sheath was placed on the mouse's tail to prevent tail climbing, and the end of the tail

1060 was secured with a piece of tape. The other end of this piece of tape was wrapped around a
1062 wooden dowel. Behavior was recorded for 6.5 minutes. TTL pulses were delivered every 30
1064 seconds to the photometry system via the video recording computer to allow alignment between
behavior and photometry signals. The same TTL setup was used to align OFT behavior with
photometry.

1066 **Histology & Immunohistochemistry**

1068 Following completion of experiments, mice were anesthetized with isoflurane and transcardially
1068 perfused with 15mL of 0.1M phosphate-buffered saline (PBS, Gibco Sciences) followed by 15mL
1070 of 4% paraformaldehyde (PFA, Sigma) in PBS. Brains were dissected from the skull and post-
1070 fixed in PFA for 24 hours, after which they were transferred to either PBS + 0.01% sodium azide
1072 (for vibratome sectioning) or 30% sucrose in PBS (for cryosectioning). Once brains for
1072 cryosectioning no longer floated in 30% sucrose, brains were embedded in Optimum Cutting
1074 Temperature (OCT; Tissue Tek) and frozen at -80°C, followed by sectioning on a cryostat at
1074 60µm. Other brains were sectioned on a vibratome at 60µm in PBS. Sections were stored in
1076 cryoprotectant at -20°C until staining. For validation of fiber tracts and viral expression, sections
1076 were DAPI stained, mounted, and imaged with a 5x objective on a Leica DM6 B scanning
microscope.

1078

MORF3 Dendritic Spine Imaging

1080 Heterozygous MORF3 mice were injected with 200nL AAVrg-Ef1a-mCherry-IRES-Cre (Addgene
1080 #55632, 2.2×10^{13} vg/mL) in either claustrum/agranular insula (CLA/AI) or PAG to label dmPFC IT
1082 and PT neurons, respectively. CLA/AI was used as an IT target instead of contralateral PFC to
1082 promote sparser labeling and limit background from dense back-projecting axons. Mice were also
1084 implanted with a skull bar to allow aiTBS or sham treatment. After at least one week of recovery
1084 from surgery, mice were placed on CORT for 14 days, followed by one day of aiTBS or sham
1086 treatment. The following day, mice were perfused. Vibratome sections of these brains were
1086 collected at 60µm.

1088

1090 To stain for V5, the epitope tag used to label Cre-expressing cells in MORF3 mice, sections were
1090 washed 3 x 10 minutes in PBS, followed by 1 hour in blocking solution containing 3% Normal
1092 Donkey Serum (NDS), 3% Bovine Serum Albumin (BSA), and 0.5% Triton-X100 in PBS. Sections
1092 were then transferred to blocking solution containing primary antibody (Rabbit anti-V5, Bethyl
1094 A190-120A, 1:500) for 3 nights, shaking at 4°C. Sections were washed 3 x 10 minutes in PBS
1094 and transferred to blocking solution containing secondary antibody (Donkey anti-rabbit, Alexa 647
1096 conjugate, Jackson ImmunoResearch 711-605-152, 1:5000) for one night, shaking at 4°C.
1096 Sections were washed 3 x 10 minutes in PBS, stained with DAPI (1:4000), and mounted.

1098 Spine images were collected using a 63x oil immersion objective on a Zeiss LSM700 confocal
1098 microscope. A z-stack extending above and below the planes in which the dendrite was visible
1100 was obtained to ensure the capture of all dendritic spines. The interval between z-steps was
1100 0.45µm. At least 8 dendrites were collected per brain, split between apical and basal dendrites.

1102

Chemogenetic Inhibition of IT Neurons

1104 To achieve bilateral inhibition of dmPFC cells in each hemisphere projecting to the contralateral
1104 hemisphere, a four-virus intersectional strategy was used. In left dmPFC, mice were injected with
1106 a mixture of 400nL AAV8-hSyn-DIO-hM4D(Gi)-mCherry (Addgene #44362, 2×10^{13} vg/mL) and
1106 200nL AAVrg-Ef1a-FlpO (Addgene #55637, 1.6×10^{13} vg/mL). In right dmPFC, mice were injected
1108 with a mixture of 400nL AAV8-hSyn-fDIO-hM4D(Gi)-mCherry (Addgene #154867, 2.5×10^{13}
1108 vg/mL) and 200nL AAVrg-Ef1a-Cre (Addgene #55636, 2.2×10^{13} vg/mL). Consistent with previous
1110 studies of contralaterally-projecting mPFC neurons^{71,104}, this approach yielded viral expression

1112 that was largely restricted to layers 2/3 and 5a of dmPFC, with some expression in deeper layers
1114 (Fig. 5A, S7). Control animals received AAV8-hSyn-DIO-mCherry (Addgene #50459, 2.4×10^{13}
1116 vg/mL) and AAV8-Ef1a-fDIO-mCherry (Addgene #114471, 2.3×10^{13} vg/mL) in place of Hm4Di
viruses. All mice were implanted with a skull bar to allow aiTBS or sham treatment. 4 weeks of
viral expression were allowed prior to treatment.

1118 To assess the effects of hM4Di on neuronal activity during aiTBS, mice expressing either hM4Di
1120 or mCherry were injected with CNO dihydrochloride (3.5mg/kg in 0.9% saline, Fisher Scientific
63-295-0). 20 minutes later, mice underwent one session of aiTBS treatment. 60 minutes
1122 following treatment, mice were perfused for histological analysis of neuronal activation via Fos.
60 μ m cryosections were washed 3 x 10 minutes in PBS, followed by 1 hour in blocking solution
1124 containing 10% Normal Donkey Serum (NDS) and 0.3% Triton-X100 in PBS. Sections were
transferred to blocking solution containing primary antibody (Rabbit anti-Fos, Synaptic Systems
226008, 1:1000) for 3 nights, shaking at 4°C. Sections were washed 3 x 10 minutes in PBS and
1126 transferred to blocking solution containing secondary antibody (Donkey anti-rabbit, Alexa 647
conjugate, Jackson ImmunoResearch 711-605-152, 1:1000) for 2 hours at room temperature.
1128 Sections were washed 3 x 10 minutes in PBS, stained with DAPI (1:4000), and mounted. Z stacks
with an interval of 1 μ m were collected using a 10x objective on a Leica STELLARIS confocal
microscope. Colocalization between Fos and mCherry was analyzed in ImageJ¹¹⁶.

1130 For behavioral chemogenetics experiments, mice were placed on CORT for 14 days. On the 14th
1132 day, mice underwent FST to obtain a pre-TMS baseline. The next day, mice underwent iTBS or
sham treatment. All mice were injected with 3.5mg/kg CNO 20 minutes prior to the first, fourth,
1134 and seventh sessions of iTBS. The following day, mice underwent FST as above.

1136 **QUANTIFICATION AND STATISTICAL ANALYSIS**

1138 Statistical tests were performed in GraphPad Prism. Details of statistical testing and results are
available in the figure legends and Table S1. For all experiments n represents an individual
1140 mouse. All error bars represent mean \pm SEM. Shading on photometry plots represents mean \pm SEM
calculated using the average trace from all animals in each condition. In all figures #p<0.1,
1142 *p<0.05, **p<0.01, ***p<0.001, ****p<0.0001. Data distributions were tested in Prism using
D'Agostino & Pearson, Anderson-Darling, Shapiro-Wilk, and Kolmogorov-Smirnov tests prior to
1144 application of tests assuming a normal distribution. Welch's t-test was used in place of an unpaired
t-test when the F test revealed a significant difference in variance between conditions.

1146 *Fiber Photometry Analysis*

1148 Fiber photometry analysis was performed in MATLAB based on example code provided by TDT
as previously described⁷¹. In brief, raw 1kHz recordings were downsampled by a factor of 10. The
1150 MATLAB polyfit function was used to fit a curve between the 405 and 465 signals for each
recording. The predicted 465 values based on the 405 channel were subtracted from the raw 465
1152 signal to produce the signal used for analysis. The mean and standard deviation of a period prior
to each event of interest was used to baseline the signal for each event, and the z-score based
1154 on this baseline period was calculated across each event. For recordings during TMS, the
baseline period was -2 to 0 seconds relative to the start of the stimulation train. For pavlovian
1156 stimuli, the baseline period was -10 to 0 seconds relative to the start of the tone, as we have
previously described for auditory stimuli⁷¹.

1158 For OFT and TST behaviors not time-locked to a particular stimulus, events were only analyzed
1160 if the end of the previous event occurred prior to the baseline of the next period (i.e. if the mouse
had just stopped struggling less than 5 seconds before the onset of a new struggling event, this
onset event was not analyzed because the previous event would confound the baseline activity).

1162 Baseline periods were chosen to maximize the number of included events while maintaining the
1164 ability to capture potential changes in activity prior to the start of the event. For TST, the baseline
1166 period was -5 to -2 seconds relative to the onset or offset of struggling. Baseline for OFT center
1168 entry was -20 to -15 seconds relative to entry, consistent with our previous studies of innate
avoidance behavior⁷¹. Baseline for OFT center exits was -1 to 0 seconds, as entries to the center
often lasted only 1 to 3 seconds. All behavioral epochs were annotated by an expert observer
blinded to the corresponding fiber photometry signal.

1170 All statistical analyses in Figures 2, 3, and S6 were performed by calculating the average trace
1172 for all events from each animal. Each animal's trace was separately used to calculate the area
1174 under the curve for the time interval of interest, and statistical comparisons were performed across
animals. To visualize these signals, traces from each animal were smoothed with a moving
average of 0.2 seconds, and the mean \pm SEM of all animals' average traces was plotted.

1176 For generalized linear modeling of TST behavior and photometry signals in Figure 3F, the z-score
1178 of each animal's photometry signal was calculated across the entire session. DBscorer was used
1180 to generate a plot of the change in area from each frame taken up by the mouse, which correlates
1182 with the vigor at which each mouse was struggling at any point in time. A generalized linear model
with a poisson distribution was fit for each animal using 10-fold cross validation, with the
photometry signal as the input variable and the behavior as the response variable. The cross-
validated R^2 value from this model was compared across animals.

1184 *Dendritic Spine Analysis*

1186 Spines were counted in ImageJ¹¹⁶ by an expert observer blinded to condition. The simple neurite
1188 tracer plugin¹¹⁷ was used to trace the length of the dendrite in 3D space, and the spines along the
1190 traced dendrite were counted manually by scrolling through the z stack to ensure no spines were
missed. Values are reported as the number of spines counted divided by the length of the traced
dendrite. The average value from apical and basal dendrites from each brain was used for
statistical comparisons between conditions.

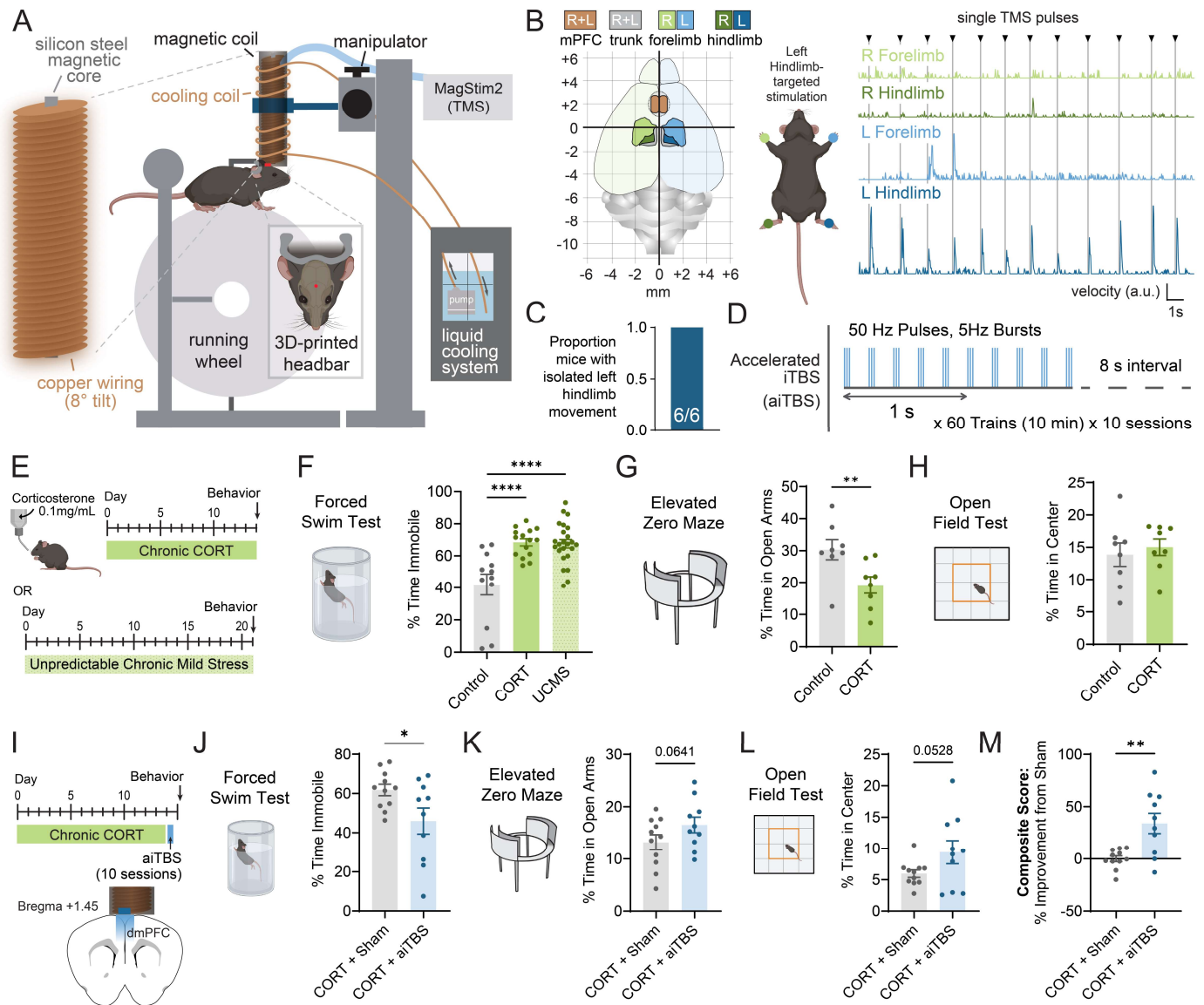


Fig. 1. Focal aiTBS over dmPFC reverses behavioral effects of chronic stress. (A) Setup for rTMS treatment. (B) Magnet focality test. Left, map of limb representation in motor cortex. Right, limb velocity upon magnetic stimulation of left hindlimb region of motor cortex. (C) Proportion of mice showing isolated left hindlimb movements upon stimulation. $n=6$ mice. (D) Accelerated iTBS protocol. (E) Timeline of stress protocols used. (F) Effects of CORT and UCMS on immobility in the forced swim test (Control $n=12$, CORT $n=15$, UCMS $n=24$ mice; one-way ANOVA with Tukey's multiple comparisons test). (G,H) Effects of CORT on anxiety-like behavior in the EZM and OFT (Control $n=8$, CORT $n=8$ mice; unpaired t-test). (I) Experimental strategy to assess behavioral effects of aiTBS treatment following chronic stress. (J, K, L) Effects of aiTBS treatment on behavior in FST, EZM, and OFT (CORT+Sham $n=11$, CORT+aiTBS $n=10$ mice; unpaired t-test). (M) Composite score of behavioral outcomes in FST, EZM, and OFT. Score was calculated as the average percent improvement from the mean of the sham-treated group across all assays (CORT+Sham $n=11$, CORT+aiTBS $n=10$ mice; unpaired t-test). Mouse diagrams were generated using Biorender.com. For detailed statistical analysis see Table S1. All error bars reflect mean \pm SEM. * $p<0.05$, ** $p<0.01$, **** $p<0.0001$.

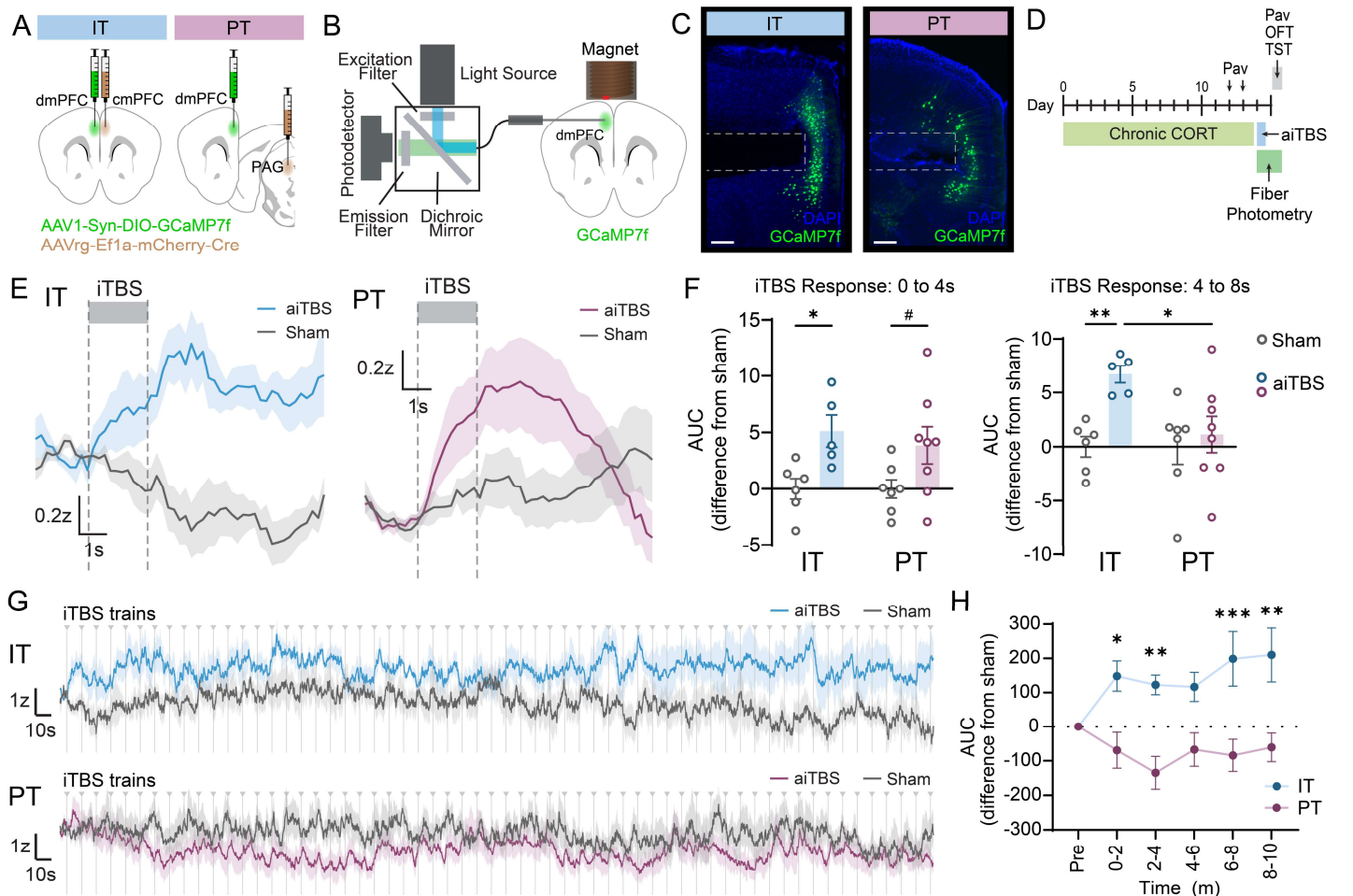


Fig. 2. aiTBS drives cell-type specific neuromodulation. (A) Viral strategy to record neural activity in IT and PT neurons of left dmPFC. (B) Fiber photometry setup with lateral fiber implant to record cell-type specific neural activity during and after rTMS. (C) Representative images of fiber placement and viral expression to record from IT and PT neurons. Scale bars 200 μ m. (D) Experimental timeline. Mice were placed on CORT for 14 days. On days 12 and 13, mice underwent Pavlovian conditioning for rewarding and aversive stimuli. On day 14, mice received aiTBS treatment, and fiber photometry signals were recorded during the first session of aiTBS. On day 15, fiber photometry signals were recorded during Pavlovian stimuli, OFT, and TST. (E) Fiber photometry recordings from IT (left) and PT (right) neurons during individual aiTBS trains. (F) Area under the curve (AUC) values calculated from plots shown in E, normalized to sham-treated mice, from IT and PT neurons during time windows relative to the start of stimulation (IT sham n=6, IT aiTBS n=5, PT sham n=7, PT aiTBS n=8 mice; two-way ANOVA with Sidak's multiple comparisons test). (G) IT and PT activity across the aiTBS session. (H) AUC values from different time bins across the session (IT sham n=6, IT aiTBS n=5, PT sham n=7, PT aiTBS n=8 mice; two-way ANOVA with Sidak's multiple comparisons test). For detailed statistical analysis see Table S1. Lines and shading reflect mean \pm SEM of average traces across mice. All error bars reflect mean \pm SEM. #p<0.1, *p<0.05, **p<0.01, ***p<0.001.

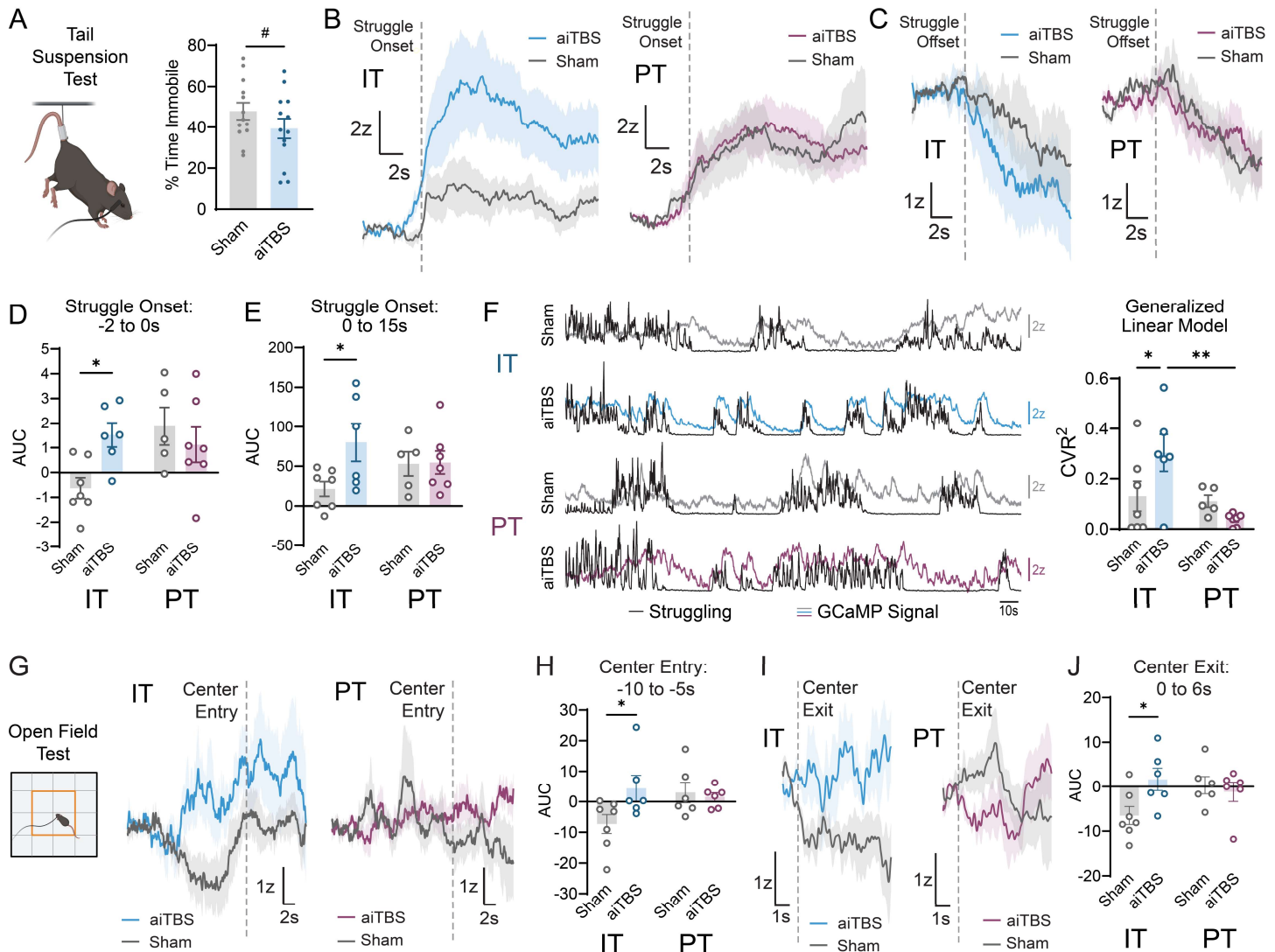


Fig. 3. Behavioral effects of aiTBS are associated with increased IT neuron activity. (A) Immobility during the first 4 minutes of TST in fiber photometry mice (Sham n=13, aiTBS n=13 mice, unpaired t-test). (B) Fiber photometry recordings of IT and PT neurons during struggling onset in mice that received aiTBS or sham treatment. (C) Same as B, but recordings of neural activity during struggling offset. (D,E) AUC values from time windows relative to struggling onset (IT sham n=7, IT aiTBS n=6, PT sham n=5, PT aiTBS n=7 mice; two-way ANOVA with Sidak's multiple comparisons test). (F) Left, representative plots showing overlay of GCaMP signal (gray or color lines) and struggling bouts during TST (black line). Right, cross-validated R² values from generalized linear models fit between photometry signals and TST behavior in each animal (IT sham n=7, IT aiTBS n=6, PT sham n=5, PT aiTBS n=7 mice; two-way ANOVA with Sidak's multiple comparisons test). (G) Fiber photometry recordings of Ca²⁺ fluorescence in IT and PT neurons prior to OFT center entry in aiTBS or sham-treated mice. (H) AUC values from -10 to -5s relative to center entry (IT sham n=7, IT aiTBS n=6, PT sham n=6, PT aiTBS n=6 mice; two-way ANOVA with Sidak's multiple comparisons test). (I) Fiber photometry recordings of Ca²⁺ fluorescence following center exits during OFT. (J) AUC values from 0 to 6s following center exit (IT sham n=7, IT aiTBS n=6, PT sham n=6, PT aiTBS n=6 mice; two-way ANOVA with Sidak's multiple comparisons test). Mouse diagrams were generated using Biorender.com. For detailed statistical analysis see Table S1. Lines and shading reflect mean \pm SEM of average traces across mice. All error bars reflect mean \pm SEM. #p < 0.1, *p < 0.05, **p < 0.01.

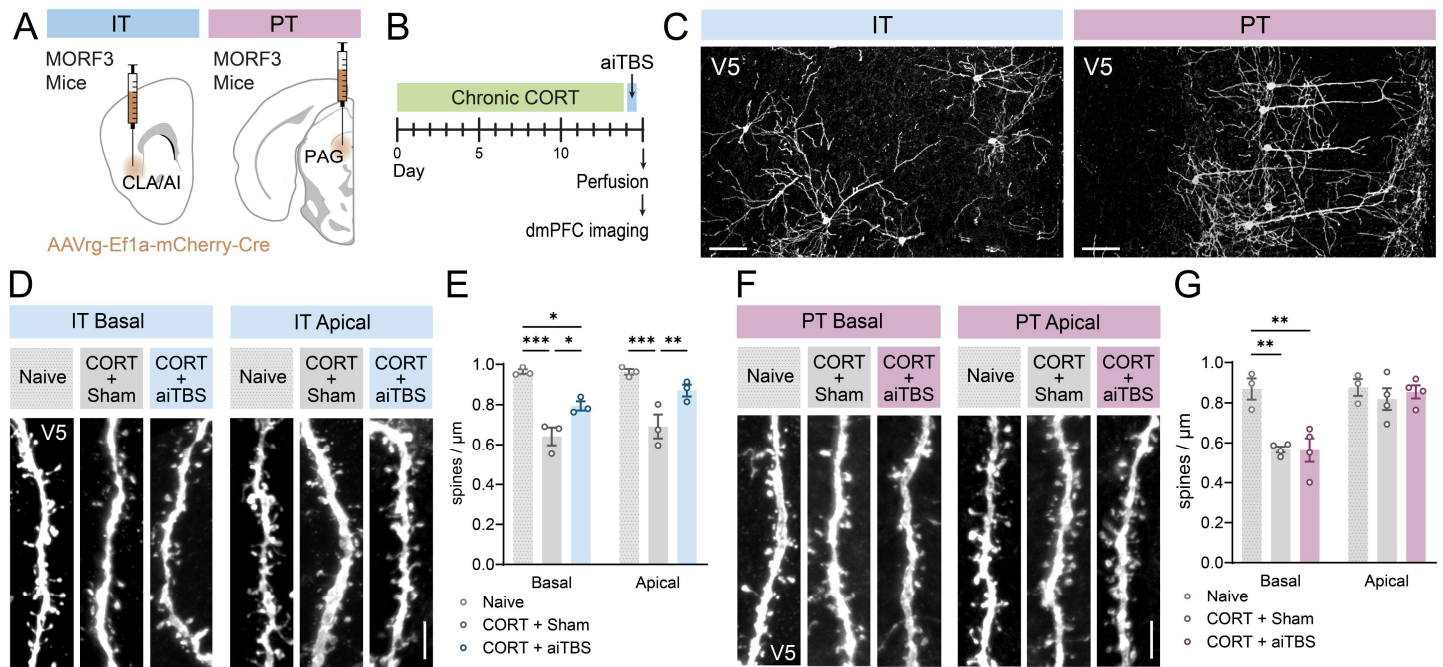


Fig. 4. aiTBS selectively elicits dendritic spine growth in IT neurons. (A) Viral strategy to achieve sparse fluorescent labeling of dmPFC IT and PT neurons in MORF3 mice. (B) Experimental timeline. Mice were placed on CORT for 14 days, followed by a day of aiTBS treatment. The day after aiTBS treatment mice were perfused for histological analysis. (C) Representative images of sparsely labeled IT and PT neurons in dmPFC of MORF3 mice. Scale bars 100 μm . (D) Representative images of dendritic spines of IT neurons in naive, CORT+sham treated, and CORT+aiTBS treated mice. Scale bar 5 μm . (E) Average dendritic spine density on IT neurons of mice from each condition (Naive n=3, CORT+sham n=3, CORT+aiTBS n=3 mice, at least 8 dendritic segments per mouse; two-way RM ANOVA with Sidak's multiple comparisons test). (F) Representative images of dendritic spines of PT neurons in naive, CORT+sham treated, and CORT+aiTBS treated mice. Scale bar 5 μm . (G) Average dendritic spine density on PT neurons of mice from each condition (Naive n=3, CORT+sham n=4, CORT+aiTBS n=4 mice, at least 8 dendritic segments per mouse; two-way RM ANOVA with Sidak's multiple comparisons test). For detailed statistical analysis see Table S1. All error bars reflect mean \pm SEM. * p <0.05, ** p <0.01, *** p <0.001.

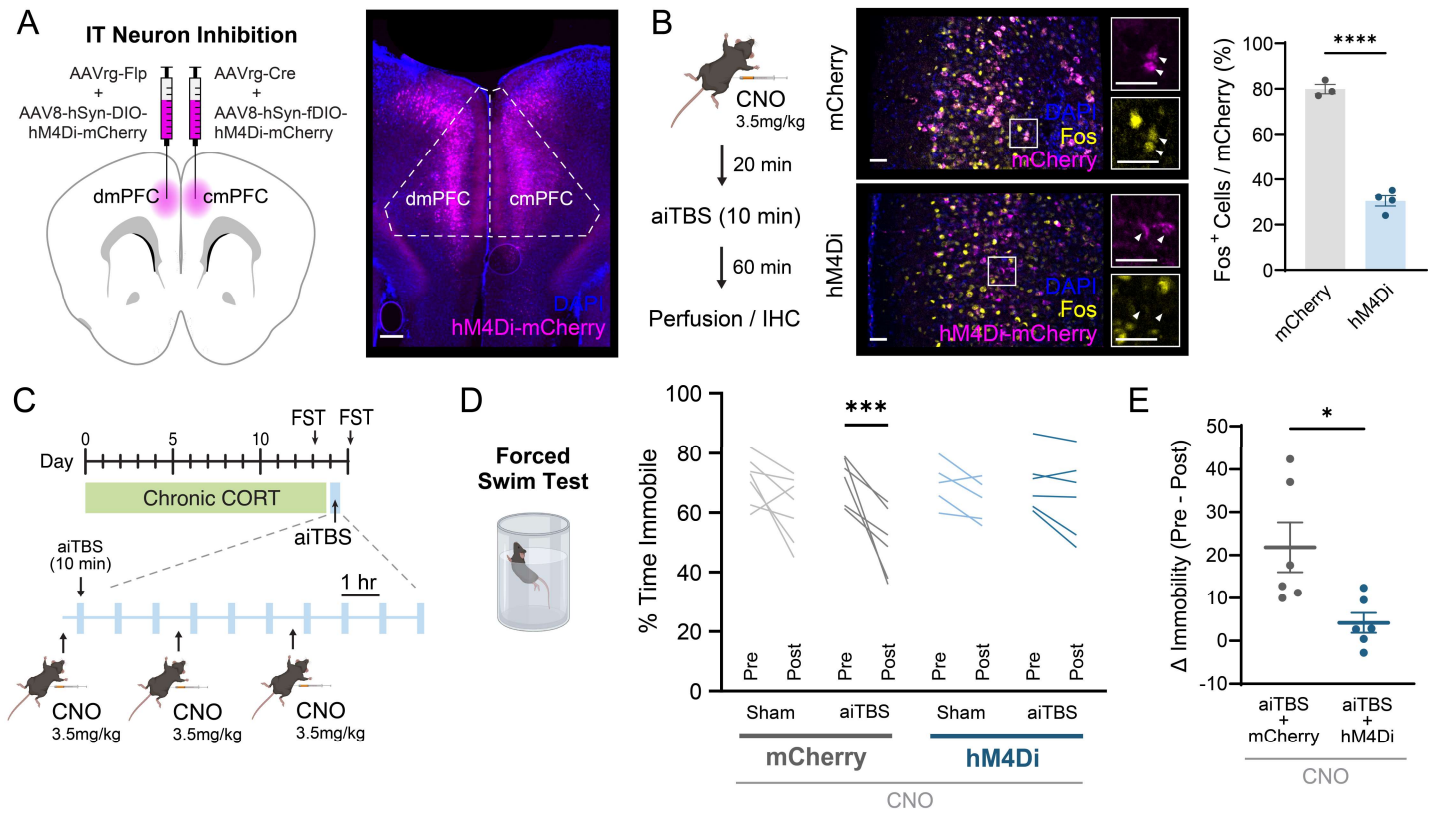


Fig. 5. Inhibition of IT neurons blocks antidepressant effects of aiTBS. (A) Left, viral strategy for cell-type specific chemogenetic inhibition of IT neurons in dmPFC. Right, representative image of hM4Di expression in dmPFC IT neurons. Scale bar 200 μ m. (B) Fos expression in dmPFC following neuronal inhibition with hM4Di. Middle, representative images of Fos and mCherry colocalization. Scale bars 40 μ m. Right, percent of mCherry⁺ neurons expressing Fos in mice expressing hM4Di (mCherry n=3, hM4Di n=4 mice; unpaired t-test). (C) Experimental strategy for inhibition of IT neurons during aiTBS. Following viral injections, mice were placed on CORT for 14 days and treated with aiTBS. Mice were injected with CNO prior to the first, fourth, and seventh aiTBS session of the day. FST was performed the day before and the day after aiTBS treatment. (D) Effects of IT neuron inhibition on immobility in the forced swim test (Sham+mCherry n=7, aiTBS+mCherry n=6, Sham+hM4Di n=5, aiTBS+hM4Di n=6 mice; three-way RM ANOVA with Sidak's multiple comparisons test). (E) Effects of IT neuron inhibition on aiTBS-induced change in immobility (aiTBS+mCherry n=6, aiTBS+hM4Di n=6 mice, unpaired t-test). Mouse diagrams were generated using Biorender.com. For detailed statistical analysis see Table S1. All error bars reflect mean \pm SEM. *p<0.05, ***p<0.001, ****p<0.0001.